Mathematical Modeling of Fluidized Bed Drying System: Review and State of the Art

Haonan Chen
Interdisciplinary Graduate School of Engineering Sciences, Kyushu University

Cheng Yang
Interdisciplinary Graduate School of Engineering Sciences, Kyushu University

Miyazaki, Takahiko
Interdisciplinary Graduate School of Engineering Sciences, Kyushu University

Young-Deuk Kim
BK21 FOUR ERICA-ACE Center, Hanyang University, 55 Hanyangdaehak-ro, Sangnok-gu, Ansan

他

https://doi.org/10.5109/7363513

出版情報：Evergreen. 12 (2), pp.1336-1368, 2025-06. Transdiscilinary Research and Education Center for Green Technologies, Kyushu University
バージョン：

Mathematical Modeling of Fluidized Bed Drying System: Review and State of the Art

Haonan Chen[1,2,*,**], Cheng Yang[1,**], Takahiko Miyazaki[1,3], Young-Deuk Kim[4,5], Muhammad Wakil Shahzad[6], Kyaw Thu[1,3,*,**]

[1]Interdisciplinary Graduate School of Engineering Sciences, Kyushu University Chikushi Campus, Kasuga-koen 6-1, Kasuga, 816-8580, Fukuoka, Japan
[2]Department of Mechanical Systems Engineering, Nagoya University, Nagoya, Furo-cho, Chikusa-ku, Nagoya, 464-8601, Japan
[3]Research Center for Next Generation Refrigerant Properties (NEXT-RP), International Institute of Carbon-Neutral Energy Research (WPI-I2CNER), Kyushu University, 744 Motooka, Nishi-ku, Fukuoka, 819-0395, Fukuoka, Japan
[4]BK21 FOUR ERICA-ACE Center, Hanyang University, 55 Hanyangdaehak-ro, Sangnok-gu, Ansan, Gyeonggido 15588, Republic of Korea
[5]Department of Mechanical Engineering, Hanyang University, 55 Hanyangdaehak-ro, Sangnok-gu, Ansan, Gyeonggi-do 15588, Republic of Korea
[6]Mechanical and Construction Engineering, Faculty of Engineering and Environment, Northumbria University, Newcastle upon Tyne, NE1 8ST, United Kingdom

*Author to whom correspondence should be addressed:
E-mail: chen.haonan.n0@f.mail.nagoya-u.ac.jp (HC); kyaw.thu.813@m.kyushu-u.ac.jp (KT)
** These authors have equal contributions to this study

(Received March 20, 2025; Revised June 25, 2025; Accepted June 26, 2025)

Abstract: Fluidized bed dryer has been widely used in chemical, food, ceramic, pharmaceutical, agriculture, polymer, and waste management industries. The fluidized drying process is a chemical or physical process affected by many factors such as fluidized velocity, particle size, and system structure. Analyzing solid particle behavior during fluidization, heat and mass transfer phenomena is essential for understanding and applying this technique. This work reviews the classification of the fluidized bed dryer and mathematical models of different systems, state of the art about modeling and simulation of the particle to predict the process and evolute the performance of different systems. As a result of this review, some traditional system structures and new hybrid systems are summarized; Zero-dimensional, one-dimensional, and CFD mathematical models are listed, which is crucial for a better understanding of fluidized bed dryers and the development of applications.

Keywords: fluidized bed; mathematical modeling; numerical simulation; drying; food industry; heat and mass transfer; particle processing

1. Fluidized bed

1.1. The Phenomenon of Fluidization

Fluidization is a process in which solid particles are transformed from a solid-like state into a fluid-like state, which occurs when a fluid (liquid or gas) is passed up through a bed of granular material [1)]. When the gas or liquid flow is introduced into the inlet of the bed of the particles, it passes through the empty spaces between particles. As shown in Figure 1, at low flow rates, inlet gas or liquid flows through the void spaces between stationary particles in a fixed bed. As the flow rate increases, the particles become suspended by the flowing gas or liquid, when the frictional force between particle and fluid equals the weight of the particles, the bed is considered to be in a state of minimum fluidization, shown in Figure 1 (b). Once the flow velocity increases above the minimum fluidization velocity, a smooth, progressive expansion occurs in the fluidized bed in a liquid-solid system, defined as smooth fluidization, as depicted in Figure 1 (c). In contrast, large instabilities with bubbling and gas

Cite: H. Chen et al., "Mathematical Modeling of Fluidized Bed Drying System: Review and State of the Art". Evergreen, 12 (02) 1336-1368 (2025). https://doi.org/10.5109/7363513.

channeling are observed in the gas-liquid system. At these higher flow rates, the movement of solids becomes more vigorous called bubbling fluidization, as shown in Figure 1 (d). Under such bubbling fluidization conditions, if the bed is deep enough and the diameter is small, the fine particles flow smoothly down by the wall around the rising gas void, called axial slugs (see Figure 1 (e)). On the other hand, the coarse particles rain down from the slug and eventually disintegrate while another slug forms at the same time, which is known as flat slugs, shown in Figure 1 (f). Once the flow velocity becomes sufficiently high, the upper surface of the bed disappears with the terminal velocity. Instead of the bubbles, a turbulent motion can be observed in the fluidized bed, see Figure 1 (g) called turbulent fluidization. With the further increase in the gas velocity, solid particles are carried out of the bed by the gas, this state is called lean phase fluidization, see Figure 1 (h).

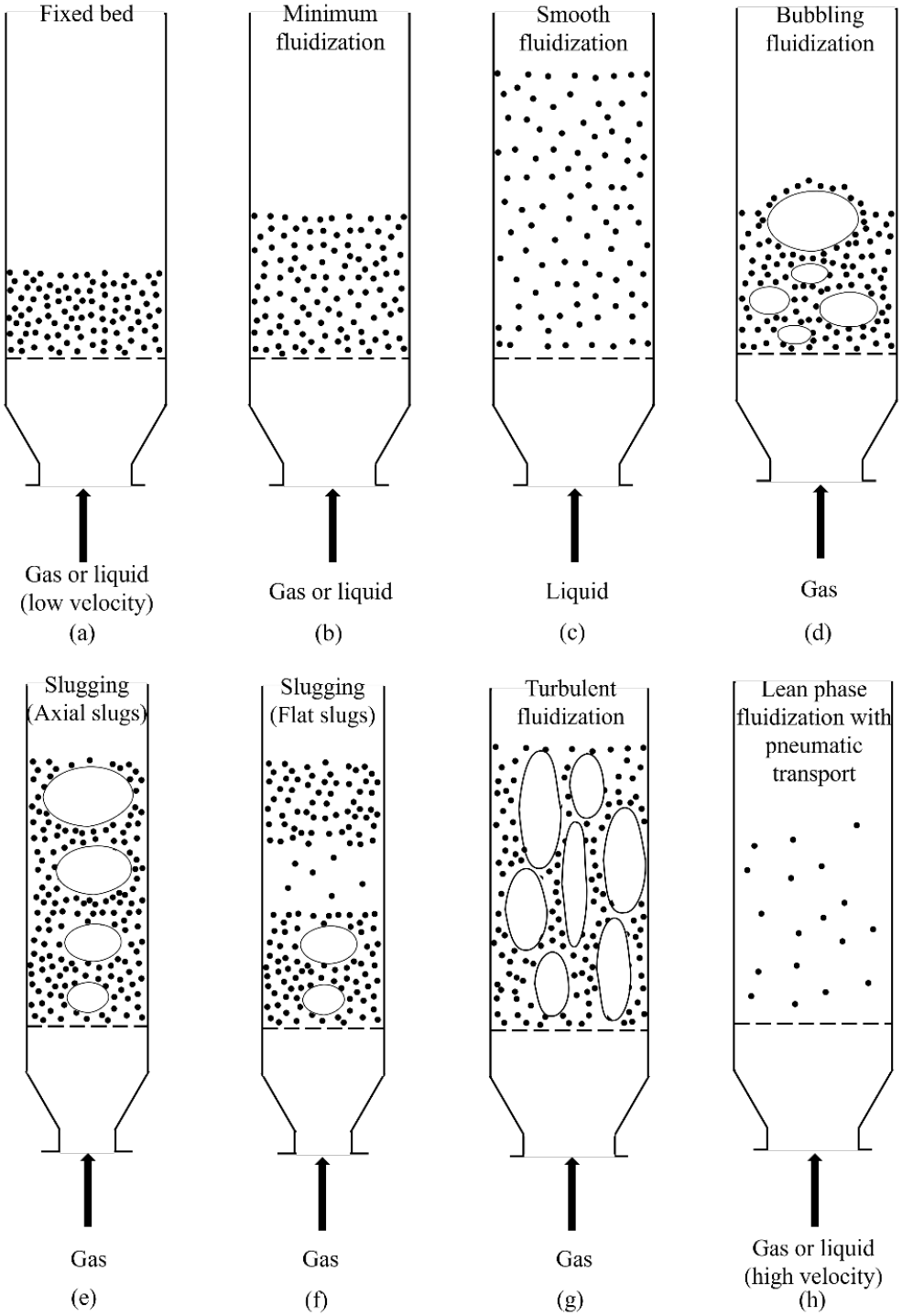

Fig. 1: Different forms of fluidization

Cite: H. Chen et al., "Mathematical Modeling of Fluidized Bed Drying System: Review and State of the Art". Evergreen, 12 (02) 1336-1368 (2025). https://doi.org/10.5109/7363513.

1.2. Particles classification and impact

Fluidization can be significantly affected by the characteristics of particles. The Geldart [2] classification of particles shown below is commonly used in many pieces of research (Figure 2).

1. Group A: Small particles with a size between 30 to 150 μm and low density (lower than 1.4 g/cm^3). These solids fluidize easily, with smooth fluidization at low gas rates.
2. Group B: Particles with a diameter of 40-500 μm and density between 1.4 and 4 g/cm^3. Which is suitable for high gas flow rates with vigorous bubbles.
3. Group C: These particles are difficult to flow with a tiny size ($d < 30\ \mu m$).
4. Group D: Fluidization of this Group particles ($d > 500\ \mu m$) is difficult, usually observable, or large and/or dense particles.

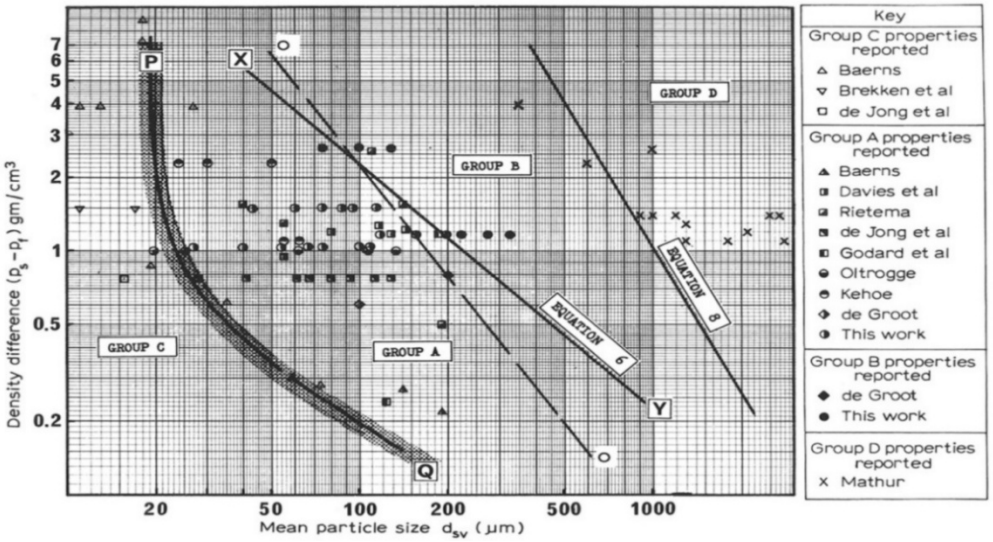

Fig. 2: The Geldart classification of particles [2]

1.3. Solid particles size

In the previous part, it was introduced that the characteristics of solid particles have a significant impact on the flow phenomenon of the fluidized bed. Therefore, in the literature and research, different solid particles usually need to choose a specific flow mode. The following Table 1 summarizes the learning of some different solid particles.

Table 1: Summary of different solid particles of Fluidized bed drying

Study	Solid particles material	size	Bed type	Ref.
Temple et al. 2000	Tea	0.8 mm	Horizontal continuous plug flow mode with 3 different temperature and pressure zones	[3]
Kaleta et al. 2013	Apple cubes	10 mm	Vertical cylinder with a diameter of 0.12 m and height of 1.80 m	[4]
Silva et al. 2012	Soybean	6 - 20 Mesh (3.36 – 0.841 mm)	Vertical acrylic tube with a diameter of 0.089 m and height of 0.7 m	[5]
Bizmark et al. 2010	Paddy	d > 0.5 mm	Horizontal type with 0.3 m length and 0.05 m width	[6]
Barathiraja et al. 2021	Turkey berry	12.8 mm	Vertical stainless-steel cone with a diameter of 0.15 m and height of 0.9 m	[7]
Ziaforoughi et al. 2016	Potato slices	3, 5 and 7 mm	PV-solar collector-assisted intermittent infrared dryer	[8]
Nazghelichi et al. 2010	Carrot cubes	4, 7 and 10 mm	Vertical Plexiglas cylinder with a diameter of 0.15 m and height of 0.3 m	[9]
Tatemoto et al. 2016	Carrot cubes, glass beads	Carrot: 20 mm glass beads: 0.106 – 0.125 mm	Vertical glass tube with an inner diameter of 0.065 m and reduced pressure	[10]

2. Fluidized bed drying

Fluidized bed has been applied to several fields, such as catalytic cracking [11], gasifiers [12] and combustors [13], chemical production and processing [14) 15], coating [16], granulation [17], and drying[18]. Among those applications, fluidized bed dryer (FBD) has been widely used in industries such as chemical [19], food [20], ceramic [21], pharmaceutical [22], agriculture [23], polymer [24], and waste management industries [25]. Fluidized beds have been proven to be successful in commercial applications [26) 27]. Table 2 compares the characteristics of fluidized bed dryer with those of traditional drying methods.

Table 2: Characteristics of fluidized bed dryer

Advantages	Limitations
High drying rates due to the high heat and mass transfer rates and smaller flow area.	High power consumption.
Higher thermal efficiency, especially if the heat source was supplied by internal heat exchanger.	Waste heat from exhaust gas has not been utilized.
Lower capital and maintenance costs.	Low flexibility and potential of fluidization if the particles are too wet.

2.1. Classification of Fluidized Bed Dryer

The simplest and most common fluidized bed dryer is a circular cross-section vessel, in which particles can be dried in either batch mode or continuously. The classification scheme of FBD available commercially was summarized in Figure 3. For a typical fluidized bed dryer, the most common operating pressure is near atmospheric, and the particulate flow regime can be divided into: [28]

a. Batch

Batch fluidized bed dryers are used for low throughput (normally < 50 kg /h and suitable for < 1000 kg/h), and multiproduct applications. Drying air is heated directly or indirectly, usually to a fixed temperature. The drying gas flow rate is also usually fixed.

b. Well-mixed

In this type of dryer, the bed temperature is uniform and is equal to the product and exhaust gas temperatures. However, due to inherent product residence time distribution, the product moisture content will span the range from inlet moisture content to a lower value.

c. Plug-flow

In plug-flow fluidized bed dryers, the bed usually has a length-to-width ratio in the range 5: 1 to 30: 1; the solids flow continuously as a plug through the channel from the inlet to the exit. This ensures approximately equal residence time for all particles, regardless of size.

The thermal behavior of batch and continuous FBD differs significantly. In batch systems, heating occurs intermittently due to the need for loading and unloading materials, typically involving heating, holding, and cooling stages. Frequent start-ups and idle periods result in higher specific energy consumption. However, the system is relatively simple, allowing for more precise thermal control and more uniform heat distribution across the product. In contrast, continuous FBD operates with steady feeding and heating, minimizing idle time and reducing energy consumption per unit of product. Nevertheless, the system is more complex due to continuous material flow and potential back-mixing. Uneven residence times can also lead to non-uniform heating, potentially compromising product quality.

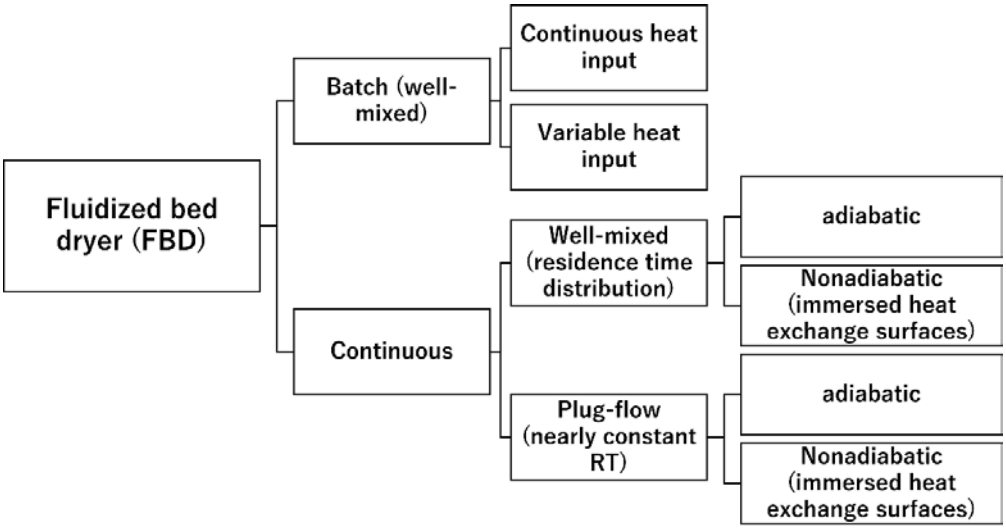

Fig. 3: A classification scheme of FBD

Cite: H. Chen et al., "Mathematical Modeling of Fluidized Bed Drying System: Review and State of the Art". Evergreen, 12 (02) 1336-1368 (2025). https://doi.org/10.5109/7363513.

2.2. System design of Fluidized Bed Dryer

2.2.1. Typical design of fluidized bed dryer

The design of conventional fluidized bed dryers is illustrated in Figure 4, (a) shows the typical single-bed dryer that is widely used in factories and laboratories for drying inorganic materials, such as dolomite or blast furnace slag. In this type of FBD, a significant fraction of the solids bypass and stays only a short time in the vessel. Figure 4. (b) provide an alternative for particles which require nearly equal drying times. Multi-stage dryer considerably narrows solid particle's residence time distribution and eliminates bypassing. Researchers have developed various mathematical models and carried out experiments to optimize the FBD drying process. Khanali et al. [29] developed a new mathematical model for predicting the plug-flow fluidized bed drying process under dynamic condition based on the previous steady-state model. Chen et al. [30] carried out several experiments and determined the residence time distribution in a continuously-operated horizontal fluidized bed. Khanali et al. [31] used a plug-flow horizontal FBD to dry shelled corn under steady-state condition by varying solid mass flow rate, drying air temperature, and weir height. Soltani et al. [32] developed an extensive experimental data set for the drying of yeast and claimed that the model could be broadly used for both laboratory and commercial scales. Sozzi et al. [33] applied a particular working condition for blackberry in a vertical bubbling FBD and achieved a drying time reduction of about 12-30 min in comparison with conventional devices. Wang et al. [34] built a prototype horizontal pulsed fluidized bed for continuous biomass torrefaction and developed a modified axial dispersion model. Table 3 summarizes the typica design of FBDs.

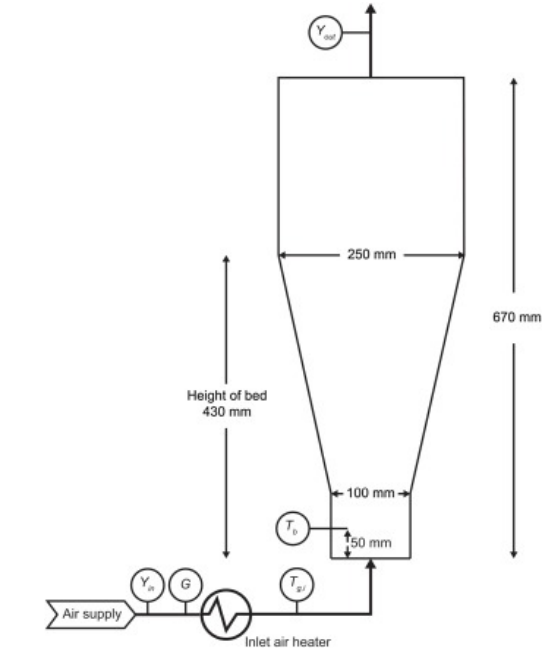

Fig. 4: Typical design of FBD: (a) schematic of the vertical fluidized bed dryer. [32]; (b) schematic of the horizontal fluidized bed dryer [30]

Table 3: Summary of typical FBD design

Study	Drying material	System design	Features	Ref.
Khanali et al. 2014	Rough rice	horizontal direction bed, plug-flow	Differential control volume method to plug-flow model for dynamic condition with mean relative error 2.1% compared to experiment solid moisture content.	[29]
Chen et al. 2017	$\gamma - Al_2O_3$ particle	horizontal direction bed	The model can only simulate particle moisture content distribution at the outlet due to current model uses given apparatus experimental data for RTDs.	[30]
Khanali et al. 2018	Shelled corn	horizontal direction bed, plug-flow	The solid moisture content decreased by increasing inlet gas temperature and weir height, whereas it increased by increasing the inlet dry solid mass flow rate.	[31]
Soltani et al. 2020	Yeast	Vertical direction bed	Model for biological materials developed in this study can be broadly applied for both laboratory and commercial scales.	[32]
Sozzi et al. 2021	Blackberry wastes	vertical direction bed, bubbling fluidized	Drying time reduction about 12-30 min in comparison with conventional devices.	[33]
Wang et al. 2022	Sawdust	horizontal pulsed bed	A modified axial dispersion model was developed.	[34]

2.2.2. Novel design of fluidized bed dryer

The design and operation of a fluidized bed dryer can significantly affect the performance and efficiency. Several novel designs and methods have been developed to improve the performance and reduce energy consumption. Solar-assisted FBD systems [35], heat pump-assisted FBD systems [36], and microwave-assisted FBD systems [37] are some of the recent developments.

Solar-assisted FBD systems utilized the solar energy to dry the products by heating up the inlet air, which can achieve the required dried capacity in some areas that do not provide sufficient sunlight. Mehran et al. [38] discussed two working conditions: natural gas drying and solar assisted drying. The result showed that solar-assisted systems have great potential to reduce energy consumption. Majumder et al. [39] investigated a novel solar assisted FBD system integrated with a dehumidifier. A solar absorber was used to regenerate the desiccant. Half an hour of the drying time can be shortened by applying the dehumidification unit. Gürel et al. [40] proposed a solar assisted FBD which uses flat plates and zigzag plates as the solar collector. This study discussed hybrid FBD system performance under a different solar collector structure.

The heat pump assisted fluidized bed dryer system uses the thermal energy obtained from the condenser to dry the product in the fluidized bed as the vapor compression or adsorption heat pump can be operated by renewable energy or waste heat, which can provide higher thermal efficiency. In recent years, several heat pump-assisted FBD systems have been proposed. Ceylan et al. [41] invented a FBD system that can switch to different working mode (solar based, heat pump based, and parabolic-trough based), system performance under different working mode had been tested by simulation and experimentally. Yahya et al. [42] use the solar collector and biomass furnace to provide heat resource and help the FBD system achieve the thermal efficiency range of 8.4% to 25.6%. Another study [43] modified the previous system by adding a multi-stage heat exchanger in order to utilize the waste heat from biomass furnace. In this study, with and without heat recovery condition have been discussed, and the result showed that thermal energy savings of 46.7% can be achieved by applying the heat recovery unit.

Microwave-assisted FBD systems combine microwave heating with conventional drying to achieve fast drying and improve thermodynamic efficiency. Microwave-assisted FBD systems have been learned by some researchers: Ranjbaran et al. [44] proved that microwave power could enhance the thermodynamic efficiency of fluidized bed dryers by a validated mathematical model. Nanvakenari et al. [45] investigate the effect of infrared and microwave power, air velocity, and temperature on the specific energy consumption, the moisture removal rate, and the product's quality in a hybrid dryer. The summary of the novel design of FBD is given in Table 4.

Table 4: Summary of novel FBD design

Study	Drying material	System design	Features	Ref.
Mehran et al. 2019	Paddy	Solar assisted, vertical direction bed	2 working condition have been discussed: natural gas drying and solar assisted drying. The result showed the potential of energy saving in the solar-assisted FBD.	[38]
Majumder et al. 2022	Ginger	Solar assisted, integrated with liquid desiccant dehumidifier.	Compared to continuous drying, intermittent drying reduced the active drying time (2–2.5 hrs.) and specific energy consumption (33.47–43.83 %) and fortified the dried ginger by reducing shrinkage (11–12 %) and increasing the Rehydration capacity (up to 22.15 %).	[39]
Gürel et al. 2022	Mint leaves	Solar assisted, vertical direction bed	The overall efficiency of the system was found to be 64%.	[40]
Ceylan et al. 2016	Mint leaves	Solar and heat pump assisted, vertical direction bed	Mixed-mode drying system. Switch between solar assisted mode, heat pump assisted mode and parabolic-trough mode.	[41]
Yahya et al. 2018	Rice	Solar, heat pump and biomass furnace assisted, vertical direction bed, in Figure 5.	The dryer decreased the moisture content of rice from 32.85% (dry basis) to 16.29% (dry basis) in 22.95 min, with a mass flow rate of 0.1037 kg/s at an average temperature of 80.9 °C and average relative humidity of 8.14%.	[42], [46]
Yahya et al. 2022	Paddy	Solar, heat pump and biomass furnace assisted, horizontal direction bed	Improve the system by using a multi-stage heat exchanger. The system reduced the paddy moisture content from 28.52% dry basis to 16.28% with a mass flow rate of 0.10328 kg/s in 23.68 min, at average temperatures of 70.3 °C.	[43]

Ranjbaran et al. 2013	Soybean	Hybrid infrared-microwave assisted.	Higher levels of air temperature led to a higher drying efficiency and decrease the exergy destruction ratio for the microwave-assisted FBD.	[44]
Nanvakenari et al. 2022	Paddy	Hybrid infrared-microwave assisted.	The experiments proved that the new hybrid system significantly increased the moisture removal rate (from 100 to 700%), head rice yield (from 5 to 40 %) and decreased the specific energy consumption (from 10 to 80%) compared to the single fluidized bed dryer.	[45]

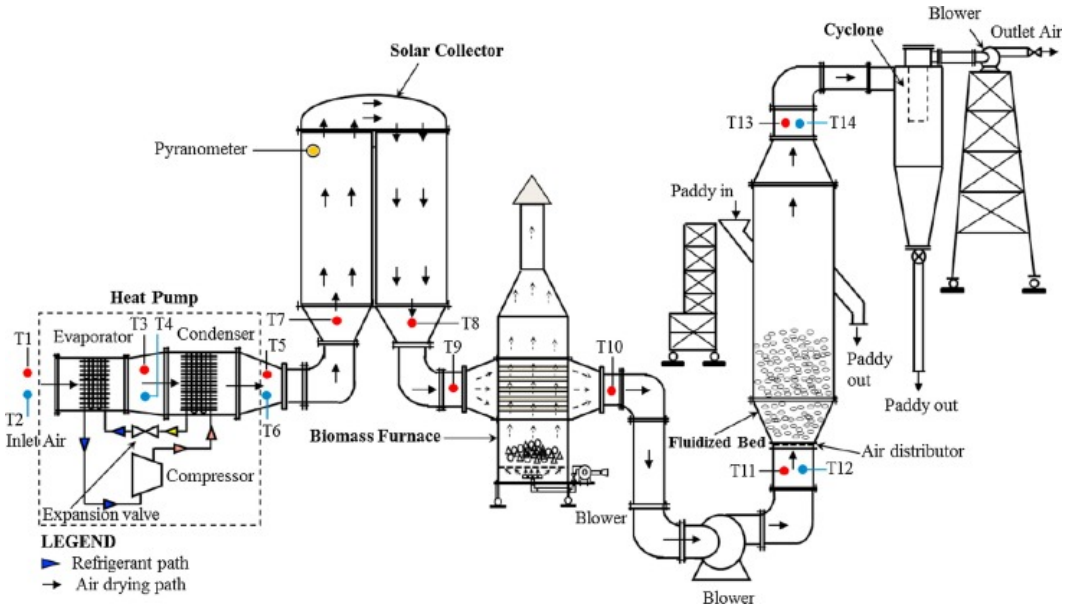

Fig. 5: Schematic of solar assisted heat pump FBD system [42]

2.3. Vibration fluidized bed dryer

The vibratory fluidized bed, due to its large drying capacity, low minimum fluidization velocity, and ability to operate continuously, is widely utilized in industrial-scale fluidized beds. Therefore, it merits a separate discussion in an additional section [47]. To enhance fluidization, various technologies were investigated, including pulsed air flow, mechanical vibration, and magnetic field or combinations of these technologies. The widely used technology on the industrial scale is the vibration of the fluidized bed. In a vibrating fluidized bed, the influence of vibration is typically quantified by the dimensionless vibration intensity Λ, which is also known as vibration strength or vibration number. The acceleration caused by vibration is determined using the frequency f and the amplitude A_f of vibration. Several experiments were conducted to investigate the drying process and system performance of the vibrating fluidized bed. Ma et al. [48] mixed the dry matter and inert particles together and learned the fluidization characteristic experimentally. The results showed that the increase in vibration intensity leads to a rise in the drying rate of vinegar residue. Lehmann et al. [49] applied the Reaction Engineering Approach (REA) to describe the drying kinetics with the assistance of experimental data. A pilot plant scale experimental setup was built by the same team [50], several conditions were carried, and the influence of parameters, including gas velocity, vibration intensity, and powder moisture content, on the fluidization characteristics of whole milk powder is studied. Meili et al. [51]tested the glass beads in a fixed bed and claimed that the fluid dynamic behavior of the bed is very dependent on the combinations of the amplitude and the frequency for the same vibration intensity. The summary of vibration fluidized bed dryer is listed in Table 5.

Table 5: Summary of vibration fluidized bed dryer

Study	Drying material	Fluidized bed characteristic	Study features	Ref.
Ma et al. 2022	vinegar residue	-	Experiment only, binary mixture included vinegar residue and inert particle (plastic particles) was putted into the bed in order to improve the fluidization. Results show that the increase of vibration intensity leads to an increase of the drying rate of vinegar residue. The addition of inert particles decreases the voidage of the bed.	48)
Lehmann et al. 2020	$\gamma - Al_2O_3$ particle; microcrystalline cellulose particle.	Batch bed.	Reaction Engineering Approach (REA) was used to describe the drying kinetics with the material specific curve. Porous particles of Geldart groups A, B and D were experimentally tested.	49)
Lehmann et al. 2019	Milk powder; glass beads.	Bubble fluidized bed.	A series of pilot plant scale experiments were carried, no mathematical model was mentioned. The influence of parameters including gas velocity, vibration intensity and powder moisture content, on the fluidization characteristics of whole milk powder is studied.	50)
Meili et al. 2012	Glass beads	Fixed bed	The results showed that the fluid dynamic behavior of the bed is very dependent on the combinations of the amplitude and the frequency for the same vibration intensity.	51)

3. Theoretical models of FBD properties

3.1. Diffusion coefficient

In the longitudinal flow fluidized bed, the flow of particles was assumed as plug flow in many cases[52), 53), 54)]. The diffusion occurs due to the moisture content differences of particles along the flow direction. Notice that the gas diffusion along the vertical path was neglected since the bed was very shallow. Nilsson et al. [53)] investigated the diffusion coefficient of particles via an experiment of sand particles and apatite granules, finding that the coefficient was affected by bed height, gas velocity, particle velocity, and particle size. Meanwhile, their experiment revealed that vibration did not significantly affect the diffusion coefficient.

$$D_m = \frac{1.49\left[0.01(H-0.05)+0.00165\rho_g\left(u_p-u_{mf}\right)\right]{u_g}^{0.23}}{u_{mf}^{1/3}} \quad (1)$$

Where H was the bed height, ρ was the density, and u was the velocity. p, g, and mf denoted the particle, gas, and minimum fluidization. For those bed heights lower than 0.1 m, Eq. (1) was simplified by Mujumdar [55)], where only particle velocity was considered.

$$D_m = \frac{3.71\times10^{-4}\left(u_p-u_{mf}\right)}{u_{mf}^{1/3}} \quad (2)$$

While for conventional FBD systems with vertical installation, well-mixed particles were laid on the distributor without any horizontal movement. Only the diffusion between vapor and air along the vertical direction was calculated [56), 49,57)]. In these cases, the diffusion coefficient was usually a function of temperature only [49,57)]

.

$$D_v = 2.6 \times 10^{-5} \cdot \left(\frac{T_p}{T_{ref}}\right)^{\frac{3}{2}} \quad (3)$$

Where T was the temperature and ref denoted the reference point. Lehmann et al. recommended using Eq. (4), with the influence of pressure [49], [58]:

$$D_v = \frac{2.252}{P} \cdot \left(\frac{T_g}{273}\right)^{1.81} \quad (4)$$

In biomass drying cases, the moisture transfer was described by effective diffusivity based on experimental data, and the diffusion coefficient was correlated via Arrhenius equation [59] [60].

$$D_e = D_0 \, exp\left(-\frac{E_a}{R_G T}\right) \quad (5)$$

Where D_0 was the diffusion coefficient at infinite temperature, E_a was the activation energy of diffusion, and R_G was the gas constant. According to frozen material drying, sublimation within the material influences the drying characteristics. Ichise and Tatemoto suggested that the diffusion coefficient should be modified, including the extra effect of Knudsen diffusion and tortuosity [61].

$$D_{\mathrm{e}} = \varepsilon^2 \left[\frac{1 - (1 - (M_w/M_{\mathrm{a}}))(P_v/P)}{D_v} + \frac{1}{Kn}\right]^{-1} \quad (6)$$

Where *M* was the molar mass, ε was the porosity, and Kn was the Knudsen coefficient. *w* and a denoted the water and the air.

3.2. Minimum Fluidization Velocity

Minimum fluidization velocity is the velocity of fluidized gas that made the whole bed suspend. The estimation was related to a dimensionless particle called Archimedes number, which is defined as the ratio of gravitational forces to viscous forces [39,56], [62,63], [1].

$$Ar = \frac{d_{\mathrm{p}}^3 \rho_g (\rho_p - \rho_g) g}{\mu_g^2} \quad (7)$$

where *dp* was particle diameter based on screen analysis, and it was more convenient to use intermediate particle diameter to determine the particle size. μ was the dynamic viscosity. In minimum fluidization velocity calculation, Kunii and Levenspiel correlation was widely applied in FBD systems [1].

$$\frac{1.75}{\varepsilon_{mf}^3 \phi_s} Re_{mf}^2 + \frac{150(1-\varepsilon_{mf})}{\varepsilon_{mf}^3 \phi_s^2} Re_{mf} = Ar \quad (8)$$

where ϕ_s was called the sphericity of particle, which defined as the ratio of the surface of sphere to the surface of the particle. And the minimum fluidization velocity was obtained from the minimum fluidization Reynolds number:

$$Re_{\mathrm{mf}} = \frac{d_p u_{mf} \rho_g}{\mu_g} \quad (9)$$

For engineering calculation, based on Eq. (8), more simplified empirical equations were adapted in minimum fluidization velocity calculation [62], [63]. Richardson correlation was described for spherical particles under automorphic pressure as [63]:

$$Re_{mf} = [25.7^2 + 0.0365Ar]^{\frac{1}{2}} - 25.7 \quad (10)$$

Paudel and Feng analyzed forty-five experiment data of inert particles: sand, alumina, and glass beads and generated a new empirical correlation [62]. They also indicate that the shape of the particle effect was less significant in the correlation.

$$Re_{mf} = [30.28^2 + 0.108Ar]^{1/2} - 30.28 \quad (11)$$

In some special cases, the minimum fluidization velocity did not rely on Archimedes number. For vast particles, where the $Re_{\mathrm{mf}} > 1000$, the minimum fluidization velocity was defined as [1]:

$$u_{mf} = \frac{d_p^2(\rho_p - \rho_g)g}{150\mu_g} \frac{\varepsilon_{mf}^3 \phi_s^2}{1-\varepsilon_{mf}} \quad (12)$$

For tiny particles, where the $Re_{\mathrm{mf}} < 20$, the minimum fluidization velocity was simplified as [1]:

$$u_{mf}^2 = \frac{d_p(\rho_p - \rho_g)g}{1.75\rho_g} \varepsilon_{mf}^3 \phi_s \quad (13)$$

Kusakabe et al. modified the minimum fluidization velocity for reduced pressure FBD system depending on the pressure difference between the top and bottom of the fluidized bed [61], [64].

$$u_{\mathrm{mf}}P_{top} = u_{\mathrm{mf}}\frac{P_{top}+P_{bottom}}{2}\left(1+\frac{32\,K_n}{3}\right) \quad (14)$$

where P was the pressure, and *Kn* was Knudsen coefficient, the same variable in Eq. (6).

3.3. Mass transfer coefficient

The mass transfer coefficient of vapor in the FBD system was derived by the Sherwood number, obtained from the relation of Reynolds number and Schmidt number [1,49,65].

$$Sh = \frac{kd_p}{D} \quad (15)$$

$$Sh = 2 + 0.6Re_p^{\frac{1}{2}}\,Sc^{\frac{1}{3}} \quad (16)$$

where *Sc* was the Schmidt number and was calculated as:

$$Sc = \frac{\mu_g}{\rho_g D} \quad (17)$$

Gunn's relation of Sherwood number contained the effect of void fraction, which was well applied in CFD simulation, especially involved bubble phase [57], [65].

$$Sh = 7 - 10\varepsilon_g + 5\varepsilon_g^2 + 0.7Re_p^{0.2}Sc^{\frac{1}{3}} + \left(1.33 - 2.4\varepsilon_g + 1.2\varepsilon_g^2\right)Re_p^{0.7}Sc^{\frac{1}{3}} \quad (18)$$

For cylindrical particles within the Reynolds number up to 1000, the Sherwood number could be calculated by Clift correlation[32], [66]:

$$\frac{Sh}{Sc^{1/5}} = 0.68\left(1+\frac{1}{ReSc}\right)Re^{0.46} \quad (19)$$

Lehmann et al. indicated that in the bubble phase FDB system, the Sherwood number was supposed to contain both laminar and turbulence items [49].

$$Sh_{lam} = 0.664 \cdot \sqrt[3]{Sc}\sqrt{Re_t} \quad (20)$$

$$Sh_{turb} = \frac{0.037 \cdot Re_t^{0.8} \cdot Sc}{1 + 2.443 \cdot Re_t^{-0.1} \cdot (Sc^{2/3} - 1)} \quad (21)$$

Notice that the *Ret* was the Reynolds number of a single particle with terminal velocity.

Cite: H. Chen et al., "Mathematical Modeling of Fluidized Bed Drying System: Review and State of the Art". Evergreen, 12 (02) 1336-1368 (2025). https://doi.org/10.5109/7363513.

$$Re_{\mathrm{t}} = 18\left(\sqrt{1+\frac{1}{9}\sqrt{Ar}}\right) - 1 \quad (22)$$

The total Sherwood number was calculated as follows:

$$Sh_{total} = 2 + \sqrt{Sh_{lam}^2 + Sh_{turb}^2} \quad (23)$$

Ichise and Tatemoto investigated spherical frozen material drying at a low temperature under reduced pressure [61]. The temperature was lower than the melt temperature. Thus, the drying process was sublimation only. The sublimation process was separated into internal and external [61,67]. $k_{i\,sl}$ was the rate coefficient of internal sublimation.

$$k_{i\,sl} = \sigma\left(\frac{9.81 R_G T_p}{2\pi M_w}\right)^{1/2} \quad (24)$$

where σ was an unknown accommodation coefficient, determined by experiment only. The external mass transfer coefficient of sublimation was related to the Prandtl number and Schmidt number:

$$k_{e\,sl} = \frac{\alpha_s}{h_v}\left(\frac{\mathrm{Pr}}{\mathrm{Sc}}\right)^{2/3} \quad (25)$$

where α_s was the heat transfer coefficient at the material's surface, and h_v was the latent heat. The Prandtl number was

$$Pr = \frac{C_{p\,g}\mu_g}{k_g} \quad (26)$$

where C_p was the specific heat capacity.

3.4. Convective Heat transfer coefficient

Heat transfer in the FBD system was divided into three parts, conduction, convection, and radiation [55]. However, only conductive and convective heat transfer had an outstanding contribution. Hear transfer coefficient of gas to particle was estimated by Nusselt number [68], [28], [69].

$$Nu = \frac{\alpha_{\mathrm{p}} d_{\mathrm{p}}}{\lambda_{\mathrm{g}}} \quad (27)$$

where α was the heat transfer coefficient, and λ was the thermal conductivity. The Nusselt number was generated

by Yang's correlations [28]:

$$Nu = 0.0282 Re_p^{1.4} Pr_g^{0.33},\ 0.1 \le Re_p \le 50 \quad (28)$$

$$Nu = 1.01\ Re_p^{0.48} Pr_g^{0.33},\ 50 \le Re_p \le 1 \times 10^4 \quad (29)$$

Similar to Eq. (18), Gunn's relation of Nusselt number contained the effect of the porosity was approximated as follows [57], [65]

$$Nu = 7 - 10\varepsilon_g + 5\varepsilon_g^2 + 0.7 Re_p^{0.2} Pr^{\frac{1}{3}} + \left(1.33 - 2.4\varepsilon_g + 1.2\varepsilon_g^2\right) Re_p^{0.7} Pr^{\frac{1}{3}} \quad (30)$$

The conductive heat transfer coefficient depended on the particle itself. The convective heat transfer is differed from wall to bed, convective heat transfer from fluidized phase to particles, and heat loss [32], [68], [70]:

$$\frac{1}{\alpha_{\text{overall}}} = \frac{1}{\alpha_{wb}} + \frac{L_{wall}}{\lambda_{wall}} + \frac{1}{\alpha_{\text{loss}}} \quad (31)$$

3.5. Drying rate

The drying rate is an essential factor in the mass transfer equations. In many pieces of research, the drying was an evaporation process driven by the humidity difference of the gas phase[32], [71]. The unit was separated toward the computing method, such as the mass of vapor per second per particle weight ([kg-water kg-dry particle-1 s-1]), particle volume ([kg m-3 s-1]), or bed area ([kg m-2 s-1]). Soltani et al. [32]suggested that toward the FBD of yeast, the driving force was the humidity difference between the external surface of the particle and the gas outlet.

$$R = k\rho_g (Y_s - Y_{\text{out}})a \quad (32)$$

where *s* and out denoted the particle surface and gas outlet. k was the mass transfer coefficient. Y was the absolute humidity, a was the specific surface area of the particle and varies with particle diameter upon on moisture content and was described by Eq. (33) [32], [72].

$$a = \frac{4\left(1 - \kappa\left((X_0 - X)/X_0\right)\right)^2}{\rho_{\text{p}} d_{p0}(1 - \varepsilon)} \quad (33)$$

where X was the moisture content of the particle. κ was the particle shrinkage coefficient. The value was 0.3 for the case of yeast. Toward inorganic particles, such as sand, the driving force became the humidity difference between the saturated gas phase and the bulk gas phase [71].

$$R = k\rho_g(Y_{sat} - \mathrm{Y})a \quad (34)$$

Here, the specific surface area of the particle was obtained by Eq. (35), depending on the critical moisture content of the particle X_{cr}.

$$\begin{cases} X \geq X_{cr} \rightarrow a = a \\ X < X_{cr} \rightarrow a = a\left(\dfrac{X}{X_{cr}}\right)^3 \end{cases} \quad (35)$$

Until the moisture of the outer surface of the particle was fully evaporated, did the shape of the particle start to change, meanwhile affecting the specific surface area. For the experimental analyzed drying rate, Khanali et al. [29] did a series of batch FBD experiments of rough rice and proposed an empirical equation, as Eq. (36):

$$R = K_1 \exp(K_2 X) \quad (36)$$

where *K1*, *K2* were functions of gas temperature and are defined as:

$$K_1 = 10^{-6}\left(0.497T_g - 159.40\right) \quad (37)$$

$$K_2 = -0.236T_g + 95.84 \quad (38)$$

For the drying rate of sublimation, the interior drying rate was calculated by Eq. (39), similar to Eq. (32), the drying rate by evaporation [61]:

$$R_{\mathrm{i\,sl}} = k_{i\,sl}a_{\mathrm{i}}(X_s - X)\rho_{p\,i} \quad (39)$$

Where $k_{i\,sl}$ was the drying rate of internal sublimation by Eq. (24). Surface (external) sublimation drying rate was calculated as follows:

$$R_{\mathrm{e\,sl}} = k_{e\,sl}a_e(Y_s - Y) \quad (40)$$

where a_e was the effective sublimation area affected by the moisture content of material surface [61]:

$$\begin{cases} a_e = 1.0, & X_s \geq 0.10 \\ a_e = X_s/0.10, & X_s < 0.10 \end{cases} \quad (41)$$

3.6. Pressure drop

For upwardly and laterally directed flow in vertical FDB systems, the pressure drop across the distributor must exceed 30% of the total pressure drop across the bed [28]. Along the direction of bed height, the pressure drop was obtained by Ergun's equation, as Eq. (42) [73]:

$$\frac{\Delta P}{H} = \frac{150\mu_g u_g (1-\varepsilon)^2}{\left(\emptyset_s d_p\right)^2 \varepsilon^3} + \frac{1.75\rho_g u_g^2 (1-\varepsilon)}{\emptyset_s d_p \varepsilon^3} \quad (42)$$

While Zarekar et al. suggested that for the FBD system with bed height expansion, when the gas velocity increased above the minimum fluidization velocity, the bed pressure drop remained constant and equal to the particle weight minus buoyancy so that the initial bed height was utilized to estimate the pressure drop [74].

$$\Delta P = H_{mf}\left(\rho_p - \rho_g\right)\left(1-\varepsilon_{mf}\right)g \quad (43)$$

3.7. Moisture content

Moisture content is a property to evaluate the water adsorption in particles. In mass transfer equations, surface moisture content was included to obtain the moisture difference. For measurable moisture content. Tu et al. calculated the surface moisture content by gas pressure and the moisture content [57,75,76]:

$$X_s = 0.622\frac{P_{sat}}{P_o - P_{sat}} f\left(X_p\right) \quad (44)$$

$$P_{sat} = 1.0 \times 10^5 exp\left(13.869 - \frac{5173}{T_p}\right) \quad (45)$$

$$f\left(X_p\right) = \begin{cases} 1, & X_p > X_{cr} \\ \dfrac{X_p^n}{\left(X_p^n + K_3\right)}, & X_p \le X_{cr} \end{cases} \quad (46)$$

where *Xcr* was the critical moisture content of the particle. *n* and *K3* were constants and equal to 3 and 0.01 respectively [77].

For unmeasurable moisture content, Soltani et al. used GAB isotherm to simulate the equilibrium moisture content, related to relative humidity in the yeast drying process [32]. The GAB isotherm, derived from the Brunauer-Emmett-Teller model, is used to describe multilayer adsorption of water molecules. It incorporates three experimentally determinable parameters that account for the strength of adsorption sites, interactions between adsorbed layers, and surface adsorption capacity, respectively. Unlike the Brunauer-Emmett-Teller model, the GAB isotherm employs relative humidity as a variable, making it more convenient for practical calculations. Due to its superior accuracy under medium to high humidity conditions, it is widely applied in the field of fluidized bed drying. Van den Berg et al. [78] and Debaste et al. [79] also proved that the GAB isotherm illustrated the water adsorption in food quite well

.

$$X_{eq} = \frac{x_m c_G k_G\, RH}{(1 - k_G\, RH)(1 - k_G\, RH + c_G k_G\, RH)} \quad (47)$$

where *RH* was the relative humidity. x_m was correspond to adsorption site of surface adsorption, k_G was related to the adsorption layers, and c_G was concerned with the surface interaction [80].

3.8. Exergy Analysis

In the analysis of second law of thermodynamics, exergy is an essential index for evaluating the maximum useful

energy than can be obtained from a system when it reaches equilibrium. The exergy is not conserved and can be destroyed or consumed during the irreversible process. The amount of destroyed exergy is proportional to the entropy generation [81) 82)]. In the case of the FBD system, the exergy efficiency during the dying process was relatively low due to significant exergy losses caused by exiting air and the utilization of only a small portion of the exergy by particles [83)].

The change in the exergy of the system includes three parts: total exergy entering, total exergy leaving, and total exergy destroyed. Ozahi and Demir analyzed the exergy change of the particle in the FBD system as follows [84)]:

$$\frac{d(Ex_2 - Ex_1)_{cv}}{dt} = \dot{E}x_{heat} - \dot{E}\boldsymbol{x}_{work} + \dot{E}x_{mass,in} - \dot{E}\boldsymbol{x}_{mass\,,\,out} - \dot{E}x_{destroyed} \quad (48)$$

In drying, the exergy of heat contained two items: the exergy changes via drying (include evaporation) and the exergy loss to the surroundings. Meanwhile, the exergy destroyed was referred to as gas entropy generation. Additionally, the exergy of work was not involved. The Eq. (48) was extended as [85)]:

$$\frac{m_p d\left(ex_{p2} - ex_{p1}\right)}{\Delta t} = -\left(1 - \frac{T_0}{T_{p,av}}\right)\dot{Q}_{dry} - \left(1 - \frac{T_0}{T_b}\right)\dot{Q}_{loss} + \dot{m}_g\left(ex_{mass,in} - ex_{mass\,,\,out}\right) - T_0\dot{S}_{gen} \quad (49)$$

where Q was the heat flux. *av*, *b* denoted average and bed. $\dot{m}_{\mathrm{g}}$ was the air flow rate, and $\dot{S}_{\mathrm{gen}}$ was the generated entropy. *ex* was the specific exergy and was calculated by Eq. (50):

$$ex = (h - h_0) - T_0(\mathrm{s} - s_0) \quad (50)$$

Combined with Eq. (50), Eq. (49) was transformed into Eq. (51)

$$\frac{m_p d\left(ex_{p2} - ex_{p1}\right)}{\Delta t} = -\left(1 - \frac{T_0}{T_{p,av}}\right)\dot{Q}_{dry} - \left(1 - \frac{T_0}{T_b}\right)\dot{Q}_{loss} + \dot{m}_g\left(h_{g1} - h_{g2}\right) - T_0\dot{m}_g\left(s_{g1} - s_{g2}\right) - T_0\dot{S}_{gen} \quad (51)$$

Equations for every item were concluded in Table 6.

Table 6: Equations of items in exergy calculation

$\dot{Q}_{dry} = \frac{d\left(m_p\left(U_{p_2} - U_{p_1}\right) + m_{w_2}U_{w_2} - m_{w_1}U_{w_1}\right)}{dt}$
$\dot{m}_a\left(h_{g1} - h_{g2}\right) = \dot{m}_g c_{p_{g,av}}(T_1 - T_2) + \dot{m}_g\left(\omega_1 h_{g_1} - \omega_2 h_{g_2}\right)$
$\dot{m}_a\left(s_{g1} - s_{g2}\right) = -\dot{m}_g\left(c_{P_{g,av}} ln\,\frac{T_2}{T_1} - R_G ln\,\frac{P_2}{P_1}\right) + \dot{m}_g\left(\omega_1 s_{g_1} - \omega_2 s_{g_2}\right)$
$S_{gen} = \frac{\dot{Q}_{loss}}{T_b} + \frac{\dot{Q}_{dry}}{T_{p,av}} + \dot{m}_g\left(c_{p_{g,av}} ln\,\frac{T_2}{T_1} - R_G ln\,\frac{P_2}{P_1} + \omega_2 s_{g_2} - \omega_1 s_{g_1}\right)$

The exergy efficiency was defined as the exergy output to the exergy input. During the drying process, the exergy output was the drying item. While the exergy input was the exergy rate of drying air [84].

$$\varepsilon = \frac{\left(1 - \frac{T_0}{T_b}\right)\dot{Q}_{dry}}{\dot{E}x_{mass,in} - \dot{E}\boldsymbol{x}_{mass\,,\,out}} \qquad (52)$$

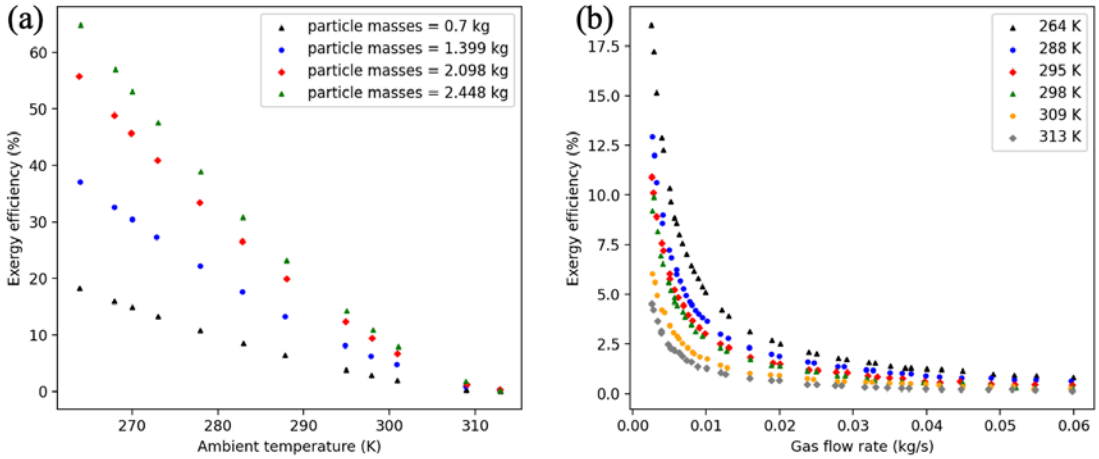

Fig. 6: Variation of exergy efficiency with respect to (a) ambient temperature with different particle masses, (b) gas flow rate with different ambient temperatures.

Figure 6 shows the effect of ambient temperature, particle masses, and gas flow rate on the exergy efficiency using the proposed model for the corn drying process [83]. Figure 6 (a) indicated that the exergy efficiency decreased with an increase in the ambient temperature, while an increase in particles mass substantially improves the exergy efficiency. Figure 6 (b) illustrates that the exergy efficiency dropped sharply when the gas mass flow rate increased. However, the change in exergy efficiency had almost the same characteristics at different ambient temperatures. Thus, it can be concluded that the effects of gas mass flow rate and particle masses are more significant than the effects of ambient air temperature on exergy efficiency.

3.9. Energy Analysis

Energy analysis, especially the energy efficiency provides an intuitive indication of the FBD system performance. Based on the first law of thermodynamics, the energy efficiency of the system is defined as the ratio of the energy transmitted to the particle to the energy input to the drying gas [85].

$$\eta = \frac{m_p\left[h_v(X_1 - X_2) + c_{p,p}\left(T_{p2} - T_{p1}\right)\right]}{\dot{m}_g\left(h_{g1} - h_{g0}\right)\Delta t} \quad (53)$$

4. Mathematical model of FBD systems

The numerical simulation model of fluidized bed is based on classical heat and mass transfer, momentum equation, and the behavior between phases is based on experimental correlations or empirical formulas. The models of hydrodynamic can be described in two different approaches: Euler-Euler approach and Euler-Lagrange approach. For numerical simulation of fluidized beds, there are two types: one is the mathematical model established by theoretical analysis, and the other is the use of CFD tools to analyze the behavior in fluidized beds.

In order to verify the feasibility of the simulation, experimental data are indispensable. This section summarized the experimental conditions and results of the above models, combined with experimental data from other literatures to illustrate the FBD system performance.

Sozzi et al. [33] explored blackberries' drying characteristics and fluidization behavior in a bubbling fluidized bed dryer at three inlet air temperatures of 50, 60, and 70 °C under the inlet air velocity of 6 m/s. The drying rate increased with the air temperature and drying time, with lower moisture content and better flowability particle. However, the optimal temperature was 60 °C, where the dried particle had high polyphenol content, high dietary fiber content, and high antioxidant capacity.

Mohseni et al. [86] also utilized the DEM-CFD method to analyze the drying process of beechwood in a horizontal vibrating fluidized bed dryer. The Lagrangian-Eulerian approach was used to investigated heat, mass, and momentum transfer between particle to the gas phase. The experiment was developed on an industrial scale vibrating dryer, which evaluated the moisture content, residence time, size distribution, and density. The experiment was repeated three times and the results agreed well with the simulation results. The production showed that increasing the inlet air temperature and velocity resulted in a higher drying rate. In addition, the vibration effect accelerated the particle's promotion, leading to the residence time and the final particle temperature. Regarding particle size distribution, smaller particles dried faster than the larger ones due to the faster heat transfer from the core to the surface.

In Taheri's study [87], the drying of red lentil seeds and the effect of botrytis selective media (BGM) were evaluated in a microwave fluidized bed dryer at four microwave powers of 0, 300, 400, and 500 W, with inlet air of 50 and 60 °C. The results showed that the diffusivity of the water inner the red lentil increased with the increase of microwave power and inlet air temperature. By applying the specific combinations of microwave power and temperature of 300W and 60 °C or 400W and 50 °C, the BGM infection ratio could be reduced by 30 % without significant loss of seed bioactivity.

In Das et al.'s work [88], the drying performance of paddy was investigated using two conical bubble fluidized beds with a cone angle of 5° and 10°, and the result was compared with a conventional one with a cone angle of 0°. The experiment was conducted at three air velocities (1.1, 1.6, 2.1 m/s) and three inlet air temperatures (55, 60, 65 °C), with bed inventories of 1 and 3 kg. The experimental study showed that the paddy drying in the conical fluidized bed dryer with a cone angle of 10° exhibited less pressure drop, less drying time, and higher nutritional contents than the other two dryers.

Saniso et al. [59] applied a microwave assisted FBD to produce steam-free parboiled rice and compared it with a conventional type. In their study, the drying rate of rice concerning moisture content was divided into two stages. The first stage was proportional, while the second stage was exponential. Microwave assistance was found to accelerate moisture diffusion only in the first stage. while also contributing to the gelatinization of the starch inside the rice kernel, resulting in a higher head rice yield. This improvement was challenging to achieve by conventional FBD.

Yan et al. [60] estimated the drying kinetics of corn in a 2D bubbling fluidized bed with a new approach that combined digital imaging techniques and electrostatic sensing to measure moisture contents, moisture diffusivities, and mass transfer coefficient of corn at different bubble locations. According to the result, the mass transfer coefficient at the interior and boundary of the bubble was higher compared to the exterior. Furthermore, increasing inlet air temperature and velocity resulted in a higher mass transfer coefficient. However, this result was unsuitable when the bubble flow transformed into a plug or slug flow.

Zhu et al. [89] explored the ultrasound technique coupled with a fluidized bed in the drying process of Ascophyllum nodosum. The drying kinetics and product quality were estimated among five methods: oven drying, conventional fluidized bed drying, airborne ultrasound-assisted fluidized bed drying, fluidized bed drying with ultrasound pre-treatment, and fluidized bed drying with hot water blanching pre-treatment. The experiment of fluidized bed drying proceeded at the inlet air temperature of 50°C, and velocity of 6.7 m/s. Based on the result, all the fluidized bed drying methods outperformed oven drying in terms of

Cite: H. Chen et al., "Mathematical Modeling of Fluidized Bed Drying System: Review and State of the Art". Evergreen, 12 (02) 1336-1368 (2025). https://doi.org/10.5109/7363513.

drying time, product quality, and energy consumption. Among fluidized bed drying methods, airborne ultrasound-assisted fluidized bed drying exhibited the best product quality in the retention of total phenolics, while conventional fluidized bed drying obtained a higher production yield.

A scaling method was used in Chen's research [90] to predict the drying profile of pharmaceutical excipients, dibasic calcium phosphate anhydrous (DCPA), in a medium-scaled fluidized bed drying unit, based on the available experimental data of a small-scaled unit under different operating conditions of initial moisture content, inlet airflow, air temperature, and load., According to their results, the initial moisture of DCPA particles did not cause a significant effect on the drying rate. Using the normalization scaling factor in inlet air temperature and velocity predicted the experiment data of the medium-scaled unit well. Still, due to the different entrance geometry, the factor via loading change gave a higher prediction than the experiment.

Perazzini et al. [91] investigated the drying kinetics of alumina particles in a vibrating fluidized bed dryer, which was mainly governed by convective mass transfer, with different amplitudes and frequencies but the same dimensionless number Γ. The empirical Page model was utilized to describe the observed drying kinetics data. In conclusion, this study found that the drying kinetics was not only depended on the dimensionless number but also on the combination of inlet air temperature, velocity, vibrating amplitudes, and frequencies.

Lan et al. [92] developed a DEM-CFD method to simulate the drying process of oil shale in a bubbling fluidized bed and a pneumatic conveying bed, where the immersion boundary method was adopted to calculate the slip-free boundary conditions of the gas phase. The drying model was at a single particle scale, where the physical properties were uniform inside the particle. The bubbling FBD model had a significant agreement compared to the experimental data. While for the pneumatic conveying bed dryer, the maximum relative errors of the particle temperature, outlet gas temperature, and moisture content in the pneumatic conveying bed were 2.2%, 2.2%, and 7.9%.

Si et al. [93] studied the drying characteristics of lignite in the microwave fluidized bed dryer in both experiment and simulation ways. The experiment was carried out in a three-stage microwave fluidization system at microwave powers ranging from 1500 to 2700 W, inlet air velocity ranging from 1.6 to 2.2 m/s, and inlet air temperature ranging from 40 to 80 °C. The simulation was based on the Euler-Euler flow method and solved by Fluent, including the drag model. The result showed that the simulation agreed with the experimental data well. Besides, increasing microwave power and air velocity would increase the drying rate and heat transfer coefficient. The summary of the case study of FBD is given in Table 7.

Table 7: Dying conditions and features of different FBD technologies

Study	System type	Product	Approach	Conditions	Comment	Ref.
Sozzi et al. 2021	Bubbling FBD	Blackberry	Experiment and simulation	Gas temperature: 50, 60, 70 ℃ Gas velocity: 6 m/s	Fluidization under the bubble regime gave better heat and mass transfer, with drying time reduction. The product had excellent physicochemical characteristics and nutrition content.	[33]
Mohseni et al. 2019	Horizontal vibrating FBD	Beechwood	Experiment and CFD simulation	Gas temperature: 210 ℃ Gas velocity: 1.6 m/s Vibrating frequency: 11 Hz Vibrating amplitude: 3 and 6 mm in two horizontal and vertical directions	The vibration and drag force of the gas phase generated particle fluidization. The DEM-CFD simulation was applied in industrial-scaled wet biomass vibrating FBD, where operation and efficiency were optimized.	[86]
Taheri et al. 2020	Microwave FBD	Red lentil seed	Experiment	Gas temperature: 50, 60 ℃ Gas velocity: 3.2 m/s Microwave power: 0, 300, 400, 500W.	Drying and disinfection were done simultaneously by microwave FBD BGM was reduced up to 30%	[87]

Das et al. 2020	Conical bubbling FBD	Paddy	Experiment	Gas temperature: 55, 65, 75 ℃ Gas velocity: 1.1, 1.6, 2.1 m/s Cone angle: 0, 5, 10°.	High gas velocity reduced the drying time. Conical bubbling FBD narrowed the drying time and consumed less energy than the conventional one. Nutrition content decreased with the increasing trying time.	88)
Saniso et al. 2020	Microwave FBD	Paddy	Experiment and CFD simulation	Gas temperature: 111, 130, 149, 169 ℃ Gas velocity: 4.6 m/s Microwave power: 800W.	The microwave FBD, as a substitute method for providing steam-free preboiled rice, had a faster drying rate and better starch generation.	59)
Tu et al. 2023	Bubbling FBD	Semolina	Experiment and CFD simulation	Gas temperature: 65 ℃ Gas velocity: 2.1, 2.4 m/s	CFD simulation of wet particle, coupled with two-fluid model, was developed to investigate drying rate and bubble phase.	57)
Yan et al. 2022	Bubbling FBD	Corn	Experiment	Gas temperature: 45, 52, 60, 67, 75 ℃ Gas velocity: 0.31, 0.37, 0.43, 0.49, 0.56 m/s	The drying kinetics and mass transfer of biomass in bubble phase was evaluated. The activation energy was varied in different bubble region.	60)
Zhu et al. 2023	Ultrasound FBD	Ascophyllum nodosum	Experiment	Gas temperature: 50 ℃ Gas velocity: 6.7 m/s Air-born ultrasound power: 170W	The drying kinetics, yield, energy consumption, and total phenolic content was assessed among five FBD method.	94)
Chen et al. 2018	Conical FBD	DCPA	Experiment and simulation	Gas temperature: 60, 80, 100 ℃ Gas flux of small-scaled:14, 18 m3/h. Gas flux of medium-scaled 40, 54 m3/h.	A scaling equation was developed to predict the experiment data and had good consistency in low normalization scaling factor. Initial moisture of DCPA particles did not affect the trying rate significantly.	90)
Perazzini et al. 2017	Vibrating FBD	Alumina	Experiment and simulation	Gas temperature: 40, 80 ℃. Gas Velocity: 0.8, 1.2 Umf. dimensionless number Γ: 4	The same value of Γ accounted for different drying kinetics.	91)
Lan et al. 2022	Bubbling FBD Pneumatic conveying bed dryer	Oil shale	CFD simulation	Gas temperature: 116 - 350 ℃ Gas velocity of bubbling FBD: 1.6 m/s Gas velocity of pneumatic conveying dryer: 10.44 m/s	The DEM-CFD simulation of these two bed dryers, involved with immersion boundary method, had good performance in predicting fluid flow, heat and mass transfer in industrial-scale FBD.	92)
Si et al. 2019	Microwave FBD	Lignite	Experiment and CFD simulation	Gas temperature: 40, 60, 80 ℃ Gas velocity: 1.6, 1.8, 2.0, 2.2 m/s Microwave power: 1500, 1700, 2300, 2700W.	The CFD simulation was based on Euler-Euler model and had good agreement with experiment. Heat transfer coefficient, Nusselt number and particle volume fraction was discussed.	93)

4.1. Zero-dimensional model

Figure 7 showed the proposed configuration for a vertical parallel flow fluidized bed dryer. As well known, the dry air was introduced into the drying chamber from the bottom of the fluidized bed dryer, raised to the drying region, and left the chamber from the top of the dryer through the outlet pipe. The solid particles, however, were supplied from the upper part of the dryer and accumulated at the base of the fluidized bed dryer. Once the dry air was input into the fluidized bed, the solid particles with a specific humidity entered the fluidized state. The humidity difference between the solid particles and the air led to mass transfer between the two, the moisture content of the solid particles, which was carried away by the continuous input of dry air, thus, as to achieve the purpose of drying.

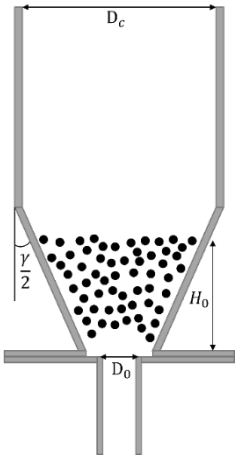

Fig. 7: Schematic diagram for a vertical fluidized bed dryer.

From a macroscopic point of view, this model took the whole of gas and solid particles as the object, and analyzed the change of its humidity and temperature with time, which was used to discuss the drying process of the fluidized bed and analyze the performance of the system. To simplify the calculation, several assumptions were given below:

1. Particle shrinkage and water diffusion within the particles were negligible.
2. The solid particles and gas mass flow rate was constant during the drying process.
3. The fluidized bed dryer behaved as a perfect mixing ideal vessel, which was considered that all the particles had the same moisture content and temperature at any time.
4. The model considered the humidity and temperature of the gas at the inlet and outlet, whereas the solid particles remained in the bed during the drying process.

The system consisted of two objects, the solid particles, and the gas. The mathematical model of the zero-dimension was established and modified based on the work by Sukunza et al. [71]. The scheme of the zero-dimensional fluidized bed dryer at dynamic conditions is outlined in Figure 8, and related equations was listed in Table 8.

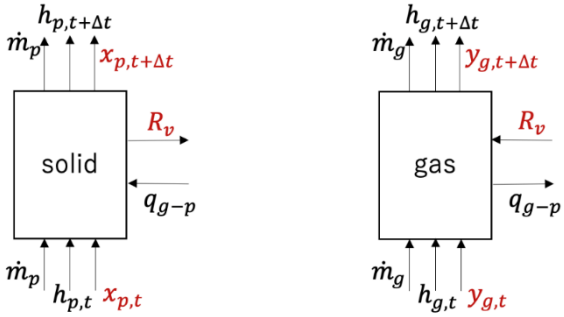

Fig. 8: Schematic diagram for the zero-dimensional fluidized bed dryer at dynamic condition.

Table 8: Zero dimension thermodynamic model of fluidized bed dryer [71]

Item	Equation	Comment
Mass balance of moisture in gas	$m_g^i \frac{dY_g^i}{dt} = \dot{m}_a(Y_g^j - Y_g^i) + R^i$ $m_g^i = \varepsilon^i V^i \rho_g$	Regard to some simulation of non-biconical particles, item of drying rate was ignored [56], [49], [84], [95].
Mass balance of moisture in particle	$m_p^i \frac{dX_p^i}{dt} = \dot{m}_p(X_p^j - X_p^i) - R^i$ $m_p^i = (1-\varepsilon^i)V^i \rho_p$	For batch fluidized bed dryer, mass flow rate of particle is zero. Thus, only item of drying rate was left on the right hand side [32].

Energy balance in the gas	$m_g^i \frac{d}{dt}\left(h_g^i + Y_g^i h_v^i\right) = \dot{m}_a\left(h_g^j + Y_g^j h_v^j - h_g^i - Y_g^i h_v^i\right) - \alpha^i a m_p^i\left(T_g^i - T_p^i\right) + R^i h_v^i - \alpha_{wall}^i\left(T_g^i - T_{amb}\right)$ $h_g^i + Y_g^i h_v^i = \left(C_{p,g} + X_p^i C_{p,v}\right)T_g^i + Y_g^i h_v^i$	Here the energy loss was not considered, but that item was widely adopted [56], [32], [84], [96].
Energy balance in the particle	$m_p^i \frac{d}{dt}\left(h_p^i + X_p^i h_w^i\right) = \dot{m}_p\left(h_p^j + X_p^j h_w^j\right) - \dot{m}_p\left(h_p^i + X_p^i h_w^i\right) + \alpha^i a m_p^i\left(T_g^i - T_p^i\right) - R^i h_v^i$ $h_p^i + X_p^i h_w^i = \left(C_{p,p} + X_p^i C_{p,w}\right)T_p^i + X_p^i h_w^i$	Mass flow rate of particle was removed for batch fluidized bed dryer. [32]
Drying rate	Refer to Eq. (34)	
Surface area	Refer to Eq. (35)	
Thermal conductivity	$\lambda_g = \lambda_{T_0}\left(\frac{T_g}{T_0}\right)^{0.9}$	
Air dynamic viscosity	$\mu_g = \mu_0\left(\frac{a}{b}\right)\left(\frac{T_g}{T_0}\right)^{3/2}$	
Specific heat capacity	$C_p = A + BT_g + CT_g^2 + DT_g^3 + \frac{E}{T_g^2}$	
Solver	ODE by stiff method	

4.2. One-dimensional model

A longitudinal plug flow FBD model was proposed by Khanali et al. [29], [97]. which based on differential equations dividing the drying bed into horizontal and vertical control volumes for particle and gas. Figure 9. shows the schematic of the longitudinal plug flow FBD. Mass and energy balances of the particles in the major control volume based on axial diffusion were developed to derive the axial distribution of particle moisture content and temperature. To derive the variation of gas moisture and temperature along the vertical direction of the fluidized bed, the axial distribution of exit gas moisture and temperature, the plug flow of the gas in the bed, and the mass and energy balance of the gas in the minor control volume were considered. Assumptions were listed as follows, and main equations were concluded in Table 9.

1. Particles were dispersed plug flow along the horizontal direction, combined with a constant bulk flow and horizontal dispersion.
2. Gas was an ideal plug flow along the vertical direction.
3. Particles were well mixed in the vertical direction.
4. The moisture content and temperature of the particles were uniform.
5. Fluidization and physical properties were constant along the horizontal direction.

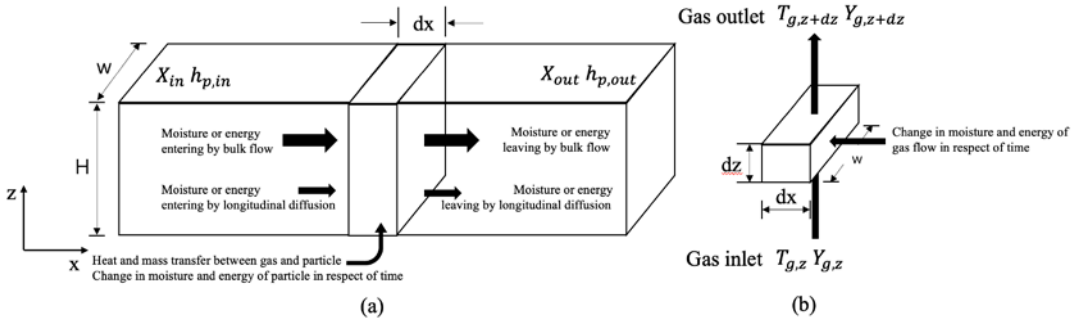

Fig. 9: Schematic diagram for the one-dimensional fluidized bed dryer at dynamic condition. (a) major control volume, (b) minor control volume

Table 9: One dimension thermodynamic model of horizontal fluidized bed dryer [29) 97)].

Item	Equation	Comment
Mass balance of moisture in gas	$u_g \frac{\partial Y}{\partial z} - \frac{R\varepsilon}{\rho_g} = -\frac{\partial Y}{\partial t}$	
Mass balance of moisture in particle	$D\frac{\partial^2 X}{\partial x^2} - u_p \frac{\partial X}{\partial x} - R = \frac{\partial X}{\partial t}$	Wang et al. developed a dispersion model in 2-D [34)]
Energy balance in the gas	$-u_g\rho_g \frac{\partial h_g}{\partial z} - a_s\alpha(T_g - T_p) + R\varepsilon\left(C_{p,w}(T_p - T_{ref}) + h_v + C_{p,v}(T_g - T_p)\right) = \rho_g \frac{\partial h_g}{\partial t}$ $h_g = (C_{p,g} + C_{p,v}Y)(T_g - T_{ref}) + Yh_v$	Here a_s was the specific surface area of the stagnant bed. While applied in the expansion bed, a_s should be replaced by a_e. please find it on the same table.
Energy balance in the particle	$D\frac{\partial^2 h_p}{\partial x^2} - u_p \frac{\partial h_p}{\partial x} + \frac{a_s\alpha(T_{g,in} - T_p)}{\varepsilon} - R\left(C_{p,w}(T_p - T_{ref}) + h_v + C_{p,v}(T_{g,in} - T_p)\right) = \frac{\partial h_p}{\partial t}$ $h_p = (C_{p,p} + C_{p,w}X)(T_p - T_{ref})$	There is another model for the Evaporative item of large particles, such as apatite [54)].
Drying rate	Refer to Eq. (36)-(38)	
Diffusion coefficient	Refer to Eq. (1)	
Minimum fluidization velocity	1.7 m/s by experiment	
Heat transfer coefficient	Refer to Eq. (27)-(29)	
specific surface area	$a = \frac{\textit{surface of all particles}}{\textit{total volume of particles in the bed}} = \frac{6(1-\varepsilon)}{\phi_s d_{sph}}$	Here the unit is [m2 m-3] [1)]
Latent heat	$h_v = 2.503\times10^6 - 2.386\times10^3(T_g - 273.16), 273.16 \le T_g \le 338.72K$ $h_v = (7.33\times10^{12} - 1.60\times10^7 T_g^2)^{0.5}, 338.72 < T_g \le 533.16K$	
Thermal conductivity	$\lambda_g = 4\times10^{-5}T_g + 0.0246$	$(T_g in ^\circ C)$
Viscosity	$\mu_g = 1.691\times10^{-5} + 4.984\times10^{-8}T_g - 3.187\times10^{-11}T_g^2 + 1.319\times10^{-14}T_g^3$	$(T_g in ^\circ C)$
Specific heat of gas	$C_{p,g} = 1009.26 - 0.0040403T_g + 6.1759\times10^{-4}T_g^2 - 4.097\times10^{-7}T_g^3$	$(T_g in ^\circ C)$
Gas density (kg/m3)	$\rho_g = 353.05/(T_g + 273.16)$	$(T_g in ^\circ C)$
Specific heat of vapor	$C_{p,v} = 1883 - 1.6737\times10^{-1}T_g + 8.4386\times10^{-4}T_g^2 - 2.6966\times10^{-7}T_g^3$	$(T_g in ^\circ C)$
Relative humidity	$RH = \frac{P_v}{P_{sat}}$	
	$P_{sat} = 100exp\left(27.0214 - 6887/(T_g + 273.16) - 5.31ln\left((T_g + 273.16)/273.16\right)\right)$	$(T_g in ^\circ C)$
Gas humidity (kg water/kg dry gas)	$Y = 0.622\frac{RH\ P_{sat}}{P_{atm} - P_{sat}}$	
Solver	MATLAB	

4.3. CFD model

Tu et al. [57] developed a CFD simulation with a two-fluid model to investigate the particle drying process in a bubbling fluidized bed, where the mass and heat transfer were divided into two phases: dense solid phase and bubble phase. The schematic was similar to Figure 7, with the 3D geometry meshed into 275,639 cells, and the 2D geometry meshed into 4,905 cells. They indicated that the drying rate was separated into a pre-heating period, a constant-rate period, and a falling-rate period. An experiment of semolina drying was established to estimate the simulation, and online electrical capacitance tomography was utilized to measure the particle concentration. Moisture content was recorded by an offline moisture meter. In their study, the particle's low moisture content increased the bubble's rising velocity. The main equations are included in Table 10, and other assumptions were as follows:

1. The bubble phase was a plug flow.
2. The cloud cover around the rising bubble was fragile.
3. The bubble phase exchanged mass and energy only with the emulsion phase.
4. The emulsion gas and solid particles were well mixed.
5. The internal mass and heat transfer of solids were negligible.
6. The particle's shape was uniform, and its physical properties were specific.
7. Collisions or agglomerations among particles were neglected.
8. The wall was adiabatic so that the heat loss was neglectable.

Table 10: CFD thermodynamic model of vertical fluidized bed dryer based on three-phase theory [57]

Item	Equation	Comment
Mass balance of gas	$\frac{\partial \varepsilon_g \rho_g}{\partial t} + \nabla \cdot \left(\varepsilon_g \rho_g \vec{u}_g\right) = \dot{m}$	In right hand site the m is mass transfer rate. For continues conditions it was replaced by zero [98]
Mass balance of particle	$\frac{\partial \varepsilon_p \rho_p}{\partial t} + \nabla \cdot \left(\varepsilon_p \rho_p \vec{u}_p\right) = -\dot{m}$	
Mass balance of moisture in gas	$\frac{\partial \left(\varepsilon_g \rho_g X_v\right)}{\partial t} + \nabla \cdot \left(\varepsilon_g \rho_g u_g X_v\right) = \nabla \cdot \left(D_v \rho_g \varepsilon_g \nabla X_v\right) + \dot{m}$	
Mass balance of moisture in particle	$\frac{\partial \left(\varepsilon_p \rho_p X_p\right)}{\partial t} + \nabla \cdot \left(\varepsilon_p \rho_p u_p X_p\right) = \nabla \cdot \left(D_v \rho_p \varepsilon_p \nabla X_p\right) - \dot{m}$	
Momentum balance of moisture in gas	$\frac{\partial \left(\varepsilon_g \rho_g \vec{u}_g\right)}{\partial t} + \nabla \cdot \left(\varepsilon_g \rho_g \vec{u}_g \vec{u}_g\right) = -\varepsilon_g \nabla P + \nabla \cdot \bar{\bar{\tau}}_g + \varepsilon_g \rho_g \vec{g} - \beta\left(\vec{u}_g - \vec{u}_p\right) + \dot{m}\vec{u}_f$	Zarekar et al. involved sub-atmospheric pressure [74]
Momentum balance of moisture in particle	$\frac{\partial \left(\varepsilon_p \rho_p \vec{u}_p\right)}{\partial t} + \nabla \cdot \left(\varepsilon_p \rho_p \vec{u}_p \vec{u}_p\right) = -\nabla \mathrm{P}_p - \varepsilon_p \nabla P + \nabla \cdot \bar{\tau}_p + \varepsilon_p \rho_p \vec{g} - \beta\left(\vec{u}_p - \vec{u}_g\right) - \dot{m}\vec{u}_p$	Collision model was widely applied [99] [94] [100]
Energy balance in the gas	$\frac{\partial \left(\varepsilon_g \rho_g h_g\right)}{\partial t} + \nabla \cdot \left(\varepsilon_g \rho_g u_g h_g\right) = -\nabla \cdot \varepsilon_g \lambda_g \nabla \mathrm{T}_g + h_t\left(T_g - T_p\right) + \tau_g \cdot \nabla \bullet u_g + \varepsilon_g \left[\frac{\partial P}{\partial t} + u_g \nabla \mathrm{P}\right] + \beta\left(u_g - u_p\right)u_g + \Delta \mathrm{h}\dot{m}$	In molten salt fluidized bed, energy dissipation was considered [101]
Energy balance in the particle	$\frac{\partial \left(\varepsilon_p \rho_p h_p\right)}{\partial t} + \nabla \cdot \left(\varepsilon_p \rho_p u_p h_p\right) = -\nabla \cdot \varepsilon_p \lambda_p \nabla \mathrm{T}_p + h_t\left(T_p - T_g\right) + \tau_p \cdot \nabla \bullet u_p + \varepsilon_p \left[\frac{\partial P}{\partial t} + u_p \nabla \mathrm{P}\right] + \beta\left(u_g - u_p\right)u_p - \Delta \mathrm{h}\dot{m}$	
Convective heat transfer rate	$\dot{q} = N_p A_{p,s} \alpha \left(T_g - T_p\right)$	
Convective mass transfer rate	$\dot{m} = N_p A_{p,s} k \left(X_s - X_g\right)$	Lan et al. differed the mass transfer into constant drying rate period and falling drying rate period [92]

Momentum transfer coefficient (gas-solid drag)	$\beta_{E_{\text{rgun}}} = 150\frac{\varepsilon_p^2\mu_g}{\varepsilon_g d_p^2} + 1.75\frac{\varepsilon_p\rho_g}{d_p}\lvert u_g - u_p\rvert \ \ \varepsilon_p > 0.8$
	$\beta_{\text{wen}-Y_u} = \frac{3}{4}C_d\frac{\varepsilon_g\varepsilon_p\rho_g}{d_p}\lvert u_g - u_p\rvert\varepsilon_g^{-2.65} \ \ \varepsilon_p \le 0.8$
Granular kinetic temperature	$\frac{3}{2}\left[\frac{\partial(\varepsilon_p\rho_p\theta)}{\partial t} + \nabla\cdot(\varepsilon_p\rho_p\theta\vec{u}_p)\right] \& = \left(-P_p I + \bar{\bar{\tau}}_p\right):\nabla\vec{u}_p + \nabla\cdot(k_p\nabla\theta) - \gamma_p + \phi_p$
Moisture content on the particle surface	Refer to Eq. (44)-(46)
Diffusion coefficient	Refer to Eq. (3)
Nusselt number	Refer to Eq. (30)
Sherwood number	Refer to Eq. (18)
Solver	Fluent

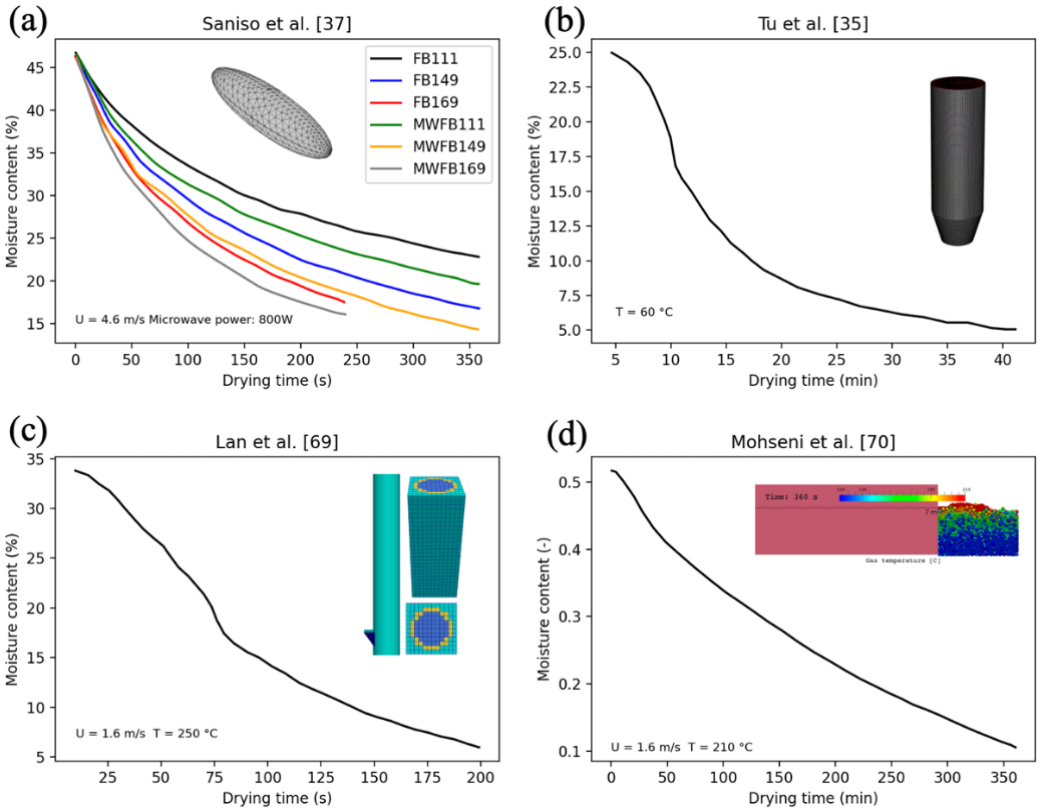

Fig. 10: CFD simulation results of moisture content with respect to drying time for (a) paddy in microwave FBD, (b) semolina in bubbling FBD, (c) oil shale in bubbling FBD, (d) beechwood in horizontal vibration FBD.

To investigate the CFD performance, four CFD simulation results of the FBD system is listed in Figure 10. Saniso et al. [59] developed an isotropic single paddy particle model using COMSOL, which was meshed into 5328 elements. The drying process was simulated using microwave FBD and ordinary FBD. Water diffusion controlled by Fick's second law, and the diffusion coefficient was related to the Arrhenius-type equation. Additionally, the deformation of the paddy during the drying process was negligible. Despite the lower operation cost, the model showed good agreement with experimental results. Tu et al. [57] conducted simulations for semolina, as shown in Figure 10 (b), with certain modifications to the assumptions and equations introduced in 2.2. They proposed two kinds of simulation in their work. The 2D CFD simulation generated the continuous drying profile of the moisture content and derived the drying rate. While 3D CFD simulations for several specific moisture values were developed to investigate the fluid dynamics, including the bubble properties and the heat and mass transfer in the whole bed. Lan et al. [92] added a linear spring-damping model in the governing equation of particles to consider the collision between particles. Figure 10 (c) printed their DEM-CFD result toward the oil shale, which showed the profile consistent with the two-stage drying rate theory. Moreover, they analyzed the Stefan Reynolds number to the drag coefficient and concluded that the Stefan effect does not influence the drag force, as well as the mass and heat transfer in the bubbling FBD system. Figure 10 (d) illustrated the drying of beechwood by vibrating FBD, based on DEM-CFD simulation using OpenFOAM. Mohseni et al. [86] applied the Hertz-Mindlin model to describe the collision impact between particles. Compared to the linear spring-damping model, the Hertz-Mindlin model was able to describe the non-linear elastic collision, which was closer to the actual condition. The simulation involved non-homogenous particle sizes, and conductive heat transfer was considered in the drying mechanism.

4.4. Experimental result

Figure 11 presented twelve experimental results of the moisture content profiles for discussing the drying process, with drying time ranged mainly from 30 min to 2 hours. For the verification experiments of CFD simulation, the experimental drying time ranged up to 6 min depending on the simulation time.

According to the profiles, the drying process could generally separate into two stages. During the first stage of the drying process, the moisture content decreased shapely, exhibiting a constant drying rate stage that appeared linearly with the drying time. For organic particles, in Figure 11 (1)-(8), this stage would last until the moisture content approaches critical moisture content, where the moisture on the particle surface is totally evaporated, and the second stage starts. In the second stage, the moisture inside the particle was transferred from the kernel to the surface. The resistance interior was not homogenous in respect of the time that slowed down the drying process, where moisture content exhibited a logarithmic relationship. This process was considered a falling drying rate stage. During the drying process under low moisture conditions, convective mass transfer from the particle to the gas phase gets weaker, but the convective heat transfer domain the process. The particle temperature increases significantly and approached the gas temperature in Soltani's research [32]. For inorganic particles in Figure 11 (9)-(12), Lan et al. [92] indicated the two-stage drying rate in the oil shale drying, while others tended to believe the drying rate was constant. Tu and Yan suggested that the drying process could divide into three stages: with a preheating stage being a period before the constant drying rate stage. Tu's experiment [57] on semolina drying was drawn in Figure 11 (6). The preheating stage was defined as the drying rate raised from 0 to the constant value which lasted for 4 min, accounting for only 10% of the total drying period. In Yan's experiment [60] on corn drying, Figure 11 (7), the moisture content was almost a horizontal line at the beginning, called the preheating stage. This stage lasted for 40 mins before constant drying started with the low inlet gas velocity lower than 0.5 m/s. The preheating stage lasts for a short time in fluidized bed dryer with high inlet air temperatures and velocities, while it lasts for a longer time in low inlet gas velocity conditions. In Figure 11 (1), increasing the inlet air temperature and velocity increases the drying rate and reduces the drying time. High inlet air temperature accelerated the heat and mass transfer of particles and gas. While high inlet air velocity caused a bubble phase in the fluidized bed that extended the interaction surface between particle and gas to strengthen the convective mass transfer. However, in Yan's experiment [60], increasing the air velocity continuously would make the bubble phase airflow turn to plug flow or slug flow, which was hostile to convective mass transfer again. Figure 11 (4) indicated that the increasing of the cone angle of the fluidized bed also benefits generating the bubble phase.

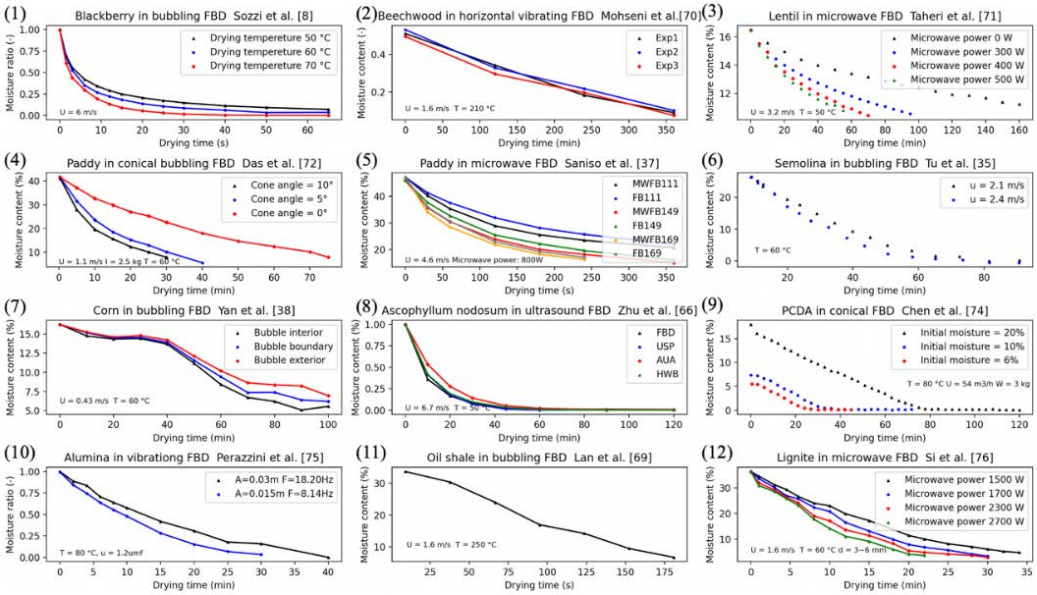

Fig. 11: Experimental result of particle moisture with respect of drying time for (1) blackberry in bubbling FBD, (2) beechwood in horizontal vibrating FBD, (3) Lentil in microwave FBD, (4) paddy in conical bubbling FBD, (5) paddy in microwave FBD, (6) semolina in bubbling FBD, (7) corn in bubbling FBD, (8) Ascophyllum nodosum in ultrasound FBD, (9) DCPA in conical FBD, (10) alumina in vibrating FBD, (11) oil shale in bubbling FBD, and (12) lignite in microwave FBD

Meanwhile, smaller particle sizes, shallower bed height, and lighter particle mass enhance the drying process. For small-size particles, the moisture evaporation distance from the kernel to the surface became shorter, so the constant drying rate period domain the drying process makes the drying process faster. Moreover, initial moisture content did not significantly affect the drying rate at the constant drying rate stage.

Conventional fluidized beds coupled with other techniques optimize fluidization conditions. Microwave-assisted fluidized bed drying was widely applied in biomass and lignite drying which was proved in Figure 11 (3), (5), and (12), where the microwave would enhance the moisture diffusion and accelerate the drying only in the constant drying rate stage. Moreover, for biomass particles, the microwave could improve the nutrition content and suppress seed disease. The vibrating fluidized bed would enhance the mass transfer and reduce u_{mf}. However, the drying kinetics with vibrating amplitudes and frequencies require further study. The ultrasound-assisted fluidized bed shows advantages in nutrition retention, drying time, and energy consumption.

5. Conclusion

Fluidized bed drying, characterized by efficient heat transfer, economical energy consumption, uniform drying, excellent product quality, and the ability to handle a wide range of materials, is a promising technology over the traditional drying method.

This review systematically introduces the principle and phenomenon of fluidization, as well as the classification of solid particles in the fluidized bed.

Mathematical models was proposed to describe the flow behavior of FBD under different operating conditions, laying the foundation of heat and mass transfer. The flow phenomena in fluidized beds are influenced by both the structure of the fluidized bed and the size of the solid particles. Therefore, this review discusses both conventional and innovative designs of fluidized bed dryer structures, as well as the size and characteristics of the solid particles used in different studies. Additionally, a method for enhancing fluidization was introduced.

In the theoretical models of fluidized bed drying (FBD), The parameters including the diffusion coefficient, minimum fluidization velocity, and drying rate, are significant indicators of thermodynamic properties. The diffusion coefficient varies depending on the type of FBD used.

Raising the gas velocity until the bubbling phase could enhance the mass transfer and reduce drying time. However, the high gas flow rate requires extensive energy input. In some case of biomass particle cases, increasing the gas velocity may result in the bubble phase reverting to the plug or slug phase again, thereby weakening the mass transfer.

Another essential parameter highlighted in this review is drying rate. The two-stage drying rate theory was widely accepted, especially for biomass particles. However, particle diameter changes' effect on the drying rate was not deeply studied. Besides, for drying kinetics, the Page model has shown good agreement with experimental data in many studies [87], [91].

For hybrid FBD systems, the vibrating FBD has the

advantages such as efficient particles mixing, reducing the minimum fluidization velocity and lowering energy consumption. Microwave-assisted FBD can accelerate the moisture diffusion and narrow the drying time. Ultrasound-assisted FBD shows good performance in preventing nutrition loss in a limited number of studies and require further exploration.

As highlighted in the reviewed literature, one of the most persistent challenges in fluidized bed dryer modeling is bridging the gap between theoretical models and practical engineering conditions:

1. The mechanisms of moisture diffusion interior of the particles still need to be unraveled. In different drying temperatures, the situation is divided into evaporation and sublimation.
2. The collision effect is difficult to be evaluated in simulation, especially the mass and conductive heat transfer in turbulence flow (bubbling phase).
3. Only a few measurement techniques can record the FBD experiment dynamically, and the experiments are not equipped with feedback control.

Thus, there still room for improvement in the design of fluidized bed dryers, which should take into account the characteristics of different materials, geometry configuration, and optimize the fluidization conditions accordingly. The drying process can also be improved by implementing feedback control systems to adjust the operating parameters based on real-time measurements of temperature, humidity and velocity. In terms of the system efficiency, several technologies can be integrated into the fluidized bed drying system such as waste heat recovery systems, which can reduce the energy consumption and operating cost. Overall, there are still challenges such as improving the accuracy of theoretical model and optimizing the design of fluidized bed dryer require further research and development.

Acknowledgment

This work was supported by the Korea Evaluation Institute of Industrial Technology (KEIT) funded by the Ministry of Trade, Industry, and Energy (MOTIE) of the Republic of Korea (No. 20018410).

Author contributions

Haonan Chen: Writing – original draft, Writing – review & editing, Conceptualization, Investigation. Cheng Yang: Writing – original draft, Writing – review & editing, Conceptualization, Investigation. Takahiko Miyazaki: Supervision, Investigation. Young-Deuk Kim: Supervision, Investigation, Funding acquisition. Muhammad Wakil Shahzad: Writing – review & editing, Supervision, Investigation. Kyaw Thu: Writing – review & editing, Conceptualization, Supervision, Investigation.

Competing interests

The authors declare that they have no known competing financial interests or personal relationships that could have appeared to influence the work reported in this paper.

Nomenclature

a	Specific surface area [m^2kg^{-1}] or [m^2 m^{-2}] or [m^2 m^{-3}]
Cp	Specific heat capacity [J kg^{-1} K^{-1}]
d	Diameter [m]
d_{sph}	Diameter of sphere having the same volume as the particle [m]
D	Diffusion coefficient [m^2 s^{-1}]
ex	Exergy [J]
E_a	Activation energy [J mol^{-1}]
G	Gravitational acceleration [m s^{-2}]
h	Enthalpy [J kg^{-1}]
h_v	Latent heat [J kg^{-1} K^{-1}]
H	Fluidized bed height [m]
k	Mass transfer coefficient [m s^{-1}]
k_i	Mass transfer coefficient of internal sublimation [m s^{-1}]
k_e	Mass transfer coefficient of external sublimation [kg m^{-2} s^{-1}]
K1	Assistant function [-]
K2	Assistant function [-]
K3	Assistant constant [-]
Kn	Knudsen coefficient [-]
L	Thickness [m]
m	Mass [kg]
$\dot{m}$	Mass flow rate [kg s^{-1}]
M	Molar mass [kg mol^{-1}]
n	Assistant constant [-]
P	Pressure [Pa]
$\dot{Q}$	Heat flux rate [kW]
R	Drying rate [kg-water kg-dry $particle^{-1}$ s^{-1}] or [kg m^{-3} s^{-1}] or [kg m^{-2} s^{-1}]
R_i	Internal sublimation drying rate [kg m^{-2} s^{-1}]
R_e	External sublimation drying rate [kg m^{-3} s^{-1}]
R_G	Gas constant [J mol^{-1} K^{-1}]
RH	Relative humidity [-]
s	Specific entropy [kJ kg^{-1} K^{-1}]
$\dot{S}$	Entropy rate [kW K^{-1}]
t	Time [s]
T	Temperature [K] or [℃]
u	Velocity [m s^{-1}]
U	Internal energy [kJ]
V	Volume [m^3]
x	x direction [m]
X	Moisture content [kg-water kg-dry $particle^{-1}$]
Y	Absolute humidity [kg-water kg-dry air^{-1}]
x_m	Parameter of adsorption site of surface [-]
c_G	Parameter of surface interaction [-]
k_G	Parameter of adsorption layers [-]
z	z direction [m]
	Greek symbols
α	Heat transfer coefficient [W m^{-2} K^{-1}]
λ	Thermal conductivity [W m^{-1} K^{-1}]

π	Ratio of circumference to diameter
σ	Accommodation coefficient
ϕ_s	Sphericity of particle [m^2 m^{-2}]
ρ	Density [kg m^{-3}]
ε	Porosity (void fraction) [-]
μ	Dynamic viscosity [kg m^{-1} s^{-1}]
κ	Shrinkage factor
	Subscripts
a	Air
atm	Atmosphere
b	Bed
bottom	Bottom of the fluidized bed
cr	Critical
e	Effective
eq	Equilibrium
es	External sublimation
g	Gas
gen	generation
i	Updated node
in	Inlet
j	Previous node
sl	sublimation
loss	Heat loss
lam	Laminar
m	Moisture of particle
mf	Minimum fluidization
s	Surface
Sat	Saturated
p	particle
$\dot{q}$	Heat flux [W s^{-1}]
ref	Reference point
out	Outlet
t	Terminal velocity
top	Top of the fluidized bed
tur	Turbulence
total	Include laminar and turbulence
v	Vapor of gas
w	Water
wb	Wall to bed
wall	Wall of vertical fluidized bed equipment
0	Initial, reference point
1	Previous state
2	Final state
	Dimensionless number
Ar	Archimedes number
Nu	Nusselt number
Pr	Prandtl number
Re	Reynolds number
Sc	Schmidt number
Sh	Sherwood number

Reference

1) D. Kunii, and O. Levenspiel, “Fluidization Engineering,” Butterworth-Heinemann, 1991.

2) D. Geldart, “Types of gas fluidization,” *Powder Technol.*, **7** (*5*) 285–292 (1973). doi:https://doi.org/10.1016/0032-5910(73)80037-3.

3) S.J. Temple, S.T. Tambala, and A.J.B. Van Boxtel, “Monitoring and control of fluid-bed drying of tea,” *Control Eng. Pract.*, **8** (*2*) 165–173 (2000). doi:10.1016/S0967-0661(99)00145-8.

4) A. Kaleta, K. Górnicki, R. Winiczenko, and A. Chojnacka, “Evaluation of drying models of apple (var. ligol) dried in a fluidized bed dryer,” *Energy Convers. Manag.*, **67** 179–185 (2013). doi:10.1016/j.enconman.2012.11.011.

5) F.R.G.B. Da Silva, M. De Souza, A.M. de S. Da Costa, L.M. de M. Jorge, and P.R. Paraíso, “Experimental and numerical analysis of soybean meal drying in fluidized bed,” *Powder Technol.*, **229** 61–70 (2012). doi:10.1016/j.powtec.2012.06.008.

6) N. Bizmark, N. Mostoufi, R. Sotudeh-Gharebagh, and H. Ehsani, “Sequential modeling of fluidized bed paddy dryer,” *J. Food Eng.*, **101** (*3*) 303–308 (2010). doi:10.1016/j.jfoodeng.2010.07.015.

7) R. Barathiraja, P. Thirumal, D. Thirumalaikumarasamy, A. Kajavali, M. Ashokkumar, and J. Thiyagaraj, “Investigation of drying kinetics and qualities of turkey berry in fluidized bed dryer,” *Mater. Today Proc.*, **46** 7711–7718 (2021). doi:10.1016/j.matpr.2021.02.217.

8) A. Ziaforoughi, and J.A. Esfahani, “A salient reduction of energy consumption and drying time in a novel pv-solar collector-assisted intermittent infrared dryer,” *Sol. Energy*, **136** 428–436 (2016). doi:10.1016/j.solener.2016.07.025.

9) T. Nazghelichi, M.H. Kianmehr, and M. Aghbashlo, “Thermodynamic analysis of fluidized bed drying of carrot cubes,” *Energy*, **35** (*12*) 4679–4684 (2010). doi:10.1016/j.energy.2010.09.036.

10) Y. Tatemoto, T. Mibu, Y. Yokoi, and A. Hagimoto, “Effect of freezing pretreatment on the drying characteristics and volume change of carrots immersed in a fluidized bed of inert particles under reduced pressure,” *J. Food Eng.*, **173** 150–157 (2016). doi:10.1016/j.jfoodeng.2015.11.006.

11) Y. Wu, S. Liu, Y. Xu, B. Lu, H. Wu, and W. Wang, “Hydrodynamic full-loop simulation of an industrial fluid catalytic cracking fluidized bed system with mechanical valves,” *Ind. Eng. Chem. Res.*, **63** (*7*) 3324–3335 (2024). doi:10.1021/acs.iecr.3c04254.

12) H. Sun, G. Bao, S. Yang, J. Hu, and H. Wang, “Numerical study of the biomass gasification process in an industrial-scale dual fluidized bed gasifier with 8mwth input,” *Renew. Energy*, **211** 681–696 (2023). doi:10.1016/j.renene.2023.04.118.

13) G. Chen, L. Shiyuan, and W. Linwei, “Current investigation status of oxy-fuel circulating fluidized bed combustion,” *Fuel*, **342** 127699 (2023). doi:10.1016/j.fuel.2023.127699.

14) D. Kim, Y. Won, B.W. Hwang, J.Y. Kim, H. Kim, Y. Choi, Y.-R. Lee, S.-Y. Lee, S.-H. Jo, Y.C. Park, J.-I. Baek, H. Nam, D. Lee, H.-J. Ryu, and J.-H. Choi, “Loop-seal flow characteristics of a circulating

fluidized bed for 3 mwth scale chemical looping combustion system," *Energy*, **274** 127271 (2023). doi:10.1016/j.energy.2023.127271.

15) G.C. Piso, P. Bareschino, P. Brachi, C. Tregambi, G. Ruoppolo, F. Pepe, and E. Mancusi, "Numerical simulation of biogas chemical looping reforming in a dual fluidized bed reactor," *Renew. Energy*, **212** 350–358 (2023). doi:10.1016/j.renene.2023.05.060.

16) Y. Song, T. Zhou, R. Bai, M. Zhang, and H. Yang, "Assessment of the coating quality in a top-spray fluidized bed coater: an experimental study," *Powder Technol.*, **439** 119663 (2024). doi:10.1016/j.powtec.2024.119663.

17) K. Vorländer, L. Bahlmann, A. Kwade, J.H. Finke, and I. Kampen, "Influence of compression kinetics during tableting of fluidized bed-granulated microorganisms on microbiological and physical-mechanical tablet properties," *Eur. J. Pharm. Biopharm.*, **188** 161–169 (2023). doi:10.1016/j.ejpb.2023.05.012.

18) S. Svetič, F. Vrečer, and K. Korasa, "Multivariate process analytical technology tools for fluidized bed granulation and drying analysis: a review," *J. Drug Deliv. Sci. Technol.*, **92** 105201 (2024). doi:10.1016/j.jddst.2023.105201.

19) A. Tahmasebi, J. Yu, Y. Han, and X. Li, "A study of chemical structure changes of chinese lignite during fluidized-bed drying in nitrogen and air," *Fuel Process. Technol.*, **101** 85–93 (2012). doi:10.1016/j.fuproc.2012.04.005.

20) I. Zahoor, A.H. Dar, K.K. Dash, R. Pandiselvam, A.V. Rusu, M. Trif, P. Singh, and G. Jeevarathinam, "Microwave assisted fluidized bed drying of bitter gourd: modelling and optimization of process conditions based on bioactive components," *Food Chem. X*, **17** 100565 (2023). doi:10.1016/j.fochx.2023.100565.

21) G.Y. Zhao, C.W. Zhu, and V. Hlavacek, "Fluidization of micron-size ceramic powders in a small-diameter fluidized bed," *Powder Technol.*, **79** (*3*) 227–235 (1994). doi:10.1016/0032-5910(94)02819-2.

22) T. Vandeputte, M. Ghijs, D. Van Hauwermeiren, E. Dos Santos Schultz, E. Schäfer, F. Stauffer, T. De Beer, and I. Nopens, "Mechanistic modeling of semicontinuous fluidized bed drying of pharmaceutical granules by incorporating single particle and bulk drying kinetics," *Int. J. Pharm.*, **646** 123447 (2023). doi:10.1016/j.ijpharm.2023.123447.

23) V.M. Korde, J.P. Giri, N.J. Giradkar, and R.B. Chadge, "Fluidised bed dryer for agricultural products: An approch," in: Recent Adv. Mater. Manuf. Mach. Learn., CRC Press, 2023.

24) S. Kumar Srivastava, M. Kumar Gupta, G. Kumar Gupta, T. Chandra Joshi, V. Shrivastava, and D. Mondal, "Fluidized spray driven polymer mediated ultra stable aluminum metal coating with enhanced dielectric properties," *Mater. Sci. Eng. B*, **294** 116490 (2023). doi:10.1016/j.mseb.2023.116490.

25) A.N.T. Tiong, and E.K.X. Lou, "Numerical study of sago pith waste drying process in a fluidised bed dryer," *Int. J. Simul. Process Model.*, **20** (*1*) 31–38 (2023). doi:10.1504/IJSPM.2023.134526.

26) S. Yoon, C. Ko, M.K. Shin, and J.M. Lee, "Experimental investigation of lab-scale fluidized bed for fine iron ore drying application under constant bed temperature condition," *Adv. Powder Technol.*, **35** (*5*) 104443 (2024). doi:10.1016/j.apt.2024.104443.

27) H.J. Das, R. Saikia, and P. Mahanta, "Thermo-economic assessment of bubbling fluidized bed paddy dryers," *Energy*, **263** 125668 (2023). doi:10.1016/j.energy.2022.125668.

28) W.-C. Yang, ed., "Handbook of Fluidization and Fluid-Particle Systems," CRC Press, Boca Raton, 2003. doi:10.1201/9780203912744.

29) M. Khanali, S. Rafiee, and A. Jafari, "Numerical simulation and experimental investigation of plug-flow fluidized bed drying under dynamic conditions," *J. Food Eng.*, **137** 64–75 (2014). doi:10.1016/j.jfoodeng.2014.03.020.

30) K. Chen, P. Bachmann, A. Bück, M. Jacob, and E. Tsotsas, "Experimental study and modeling of particle drying in a continuously-operated horizontal fluidized bed," *Particuology*, **34** 134–146 (2017). doi:10.1016/j.partic.2017.02.003.

31) M. Khanali, A. Khakpour Giglou, and S. Rafiee, "Model development for shelled corn drying in a plug flow fluidized bed dryer," *Eng. Agric. Environ. Food*, **11** (*1*) 1–8 (2018). doi:10.1016/j.eaef.2017.09.002.

32) B. Soltani, D.D. McClure, F. Oveissi, T.A.G. Langrish, and J.M. Kavanagh, "Experimental investigation and numerical modeling of pilot-scale fluidized-bed drying of yeast: part a – drying model development and validation," *Food Bioprod. Process.*, **119** 246–256 (2020). doi:10.1016/j.fbp.2019.11.008.

33) A. Sozzi, M. Zambon, G. Mazza, and D. Salvatori, "Fluidized bed drying of blackberry wastes: drying kinetics, particle characterization and nutritional value of the obtained granular solids," *Powder Technol.*, **385** 37–49 (2021). doi:10.1016/j.powtec.2021.02.058.

34) R. Wang, Z. Wang, X. Bi, C.J. Lim, and S. Sokhansanj, "Residence time distribution and solids mixing of sawdust in a horizontal pulsed fluidized bed," *Powder Technol.*, **397** 117006 (2022). doi:10.1016/j.powtec.2021.11.050.

35) P. Majumder, B. Deb, and R. Gupta, "Investigation of osmosonication pretreated chili (capsicum frutescens l.) drying in solar-assisted fluidized bed dryer utilizing dehumidified air," *J. Food Process Eng.*, **46** (*7*) e14351 (2023). doi:10.1111/jfpe.14351.

36) M. Yahya, H. Fahmi, R. Hasibuan, and A. Fudholi, "Development of hybrid solar-assisted heat pump dryer for drying paddy," *Case Stud. Therm. Eng.*, **45** 102936 (2023). doi:10.1016/j.csite.2023.102936.

37) W. Fu, Y. Zhang, L. Cui, H. Liu, and T. Maqsood, "Experimental microwave-assisted air gasification of biomass in fluidized bed reactor," *Bioresour. Technol.*, **369** 128378 (2023). doi:10.1016/j.biortech.2022.128378.

38) S. Mehran, M. Nikian, M. Ghazi, H. Zareiforoush, and I. Bagheri, "Experimental investigation and energy analysis of a solar-assisted fluidized-bed dryer including solar water heater and solar-powered infrared lamp for paddy grains drying," *Sol. Energy*, **190** (*March*) 167–184 (2019). doi:10.1016/j.solener.2019.08.002.

39) P. Majumder, B. Deb, R. Gupta, and S.S. Sablani, "A comprehensive review of fluidized bed drying: sustainable design approaches, hydrodynamic and thermodynamic performance characteristics, and product quality," *Sustain. Energy Technol. Assess.*, **53** 102643 (2022). doi:10.1016/j.seta.2022.102643.

40) A.E. Gürel, Ü. Ağbulut, A. Ergün, İ. Ceylan, A. Sözen, A.D. Tuncer, and A. Khanlari, "A detailed investigation of the temperature-controlled fluidized bed solar dryer: a numerical, experimental, and modeling study," *Sustain. Energy Technol. Assess.*, **49** (*June 2021*) 101703 (2022). doi:10.1016/j.seta.2021.101703.

41) I. Ceylan, and A.E. Gürel, "Solar-assisted fluidized bed dryer integrated with a heat pump for mint leaves," *Appl. Therm. Eng.*, **106** 899–905 (2016). doi:10.1016/j.applthermaleng.2016.06.077.

42) M. Yahya, H. Fahmi, A. Fudholi, and K. Sopian, "Performance and economic analyses on solar-assisted heat pump fluidised bed dryer integrated with biomass furnace for rice drying," *Sol. Energy*, **174** (*May*) 1058–1067 (2018). doi:10.1016/j.solener.2018.10.002.

43) M. Yahya, A. Rachman, and R. Hasibuan, "Performance analysis of solar-biomass hybrid heat pump batch-type horizontal fluidized bed dryer using multi-stage heat exchanger for paddy drying," *Energy*, **254** 124294 (2022). doi:10.1016/j.energy.2022.124294.

44) M. Ranjbaran, and D. Zare, "Simulation of energetic- and exergetic performance of microwave-assisted fluidized bed drying of soybeans," *Energy*, **59** 484–493 (2013). doi:10.1016/j.energy.2013.06.057.

45) S. Nanvakenari, K. Movagharnejad, and A. Latifi, "Modelling and experimental analysis of rice drying in new fluidized bed assisted hybrid infrared-microwave dryer," *Food Res. Int.*, **159** (*June*) 111617 (2022). doi:10.1016/j.foodres.2022.111617.

46) M. Yahya, A. Fudholi, and K. Sopian, "Energy and exergy analyses of solar-assisted fluidized bed drying integrated with biomass furnace," *Renew. Energy*, **105** 22–29 (2017). doi:10.1016/j.renene.2016.12.049.

47) M. Aghbashlo, R. Sotudeh-Gharebagh, R. Zarghami, A.S. Mujumdar, and N. Mostoufi, "Measurement techniques to monitor and control fluidization quality in fluidized bed dryers: a review," *Dry. Technol.*, **32** (*9*) 1005–1051 (2014). doi:10.1080/07373937.2014.899250.

48) C. Ma, H. Xu, W. Zhong, W. Wang, and H. Zhang, "Experimental study on fluidization characteristics of vinegar residue in a vibrated fluidized bed," *Adv. Powder Technol.*, **33** (*8*) 103698 (2022). doi:10.1016/j.apt.2022.103698.

49) S.E. Lehmann, T. Oesau, A. Jongsma, F. Innings, and S. Heinrich, "Material specific drying kinetics in fluidized bed drying under mechanical vibration using the reaction engineering approach," *Adv. Powder Technol.*, **31** (*12*) 4699–4713 (2020). doi:10.1016/j.apt.2020.11.006.

50) S.E. Lehmann, E.U. Hartge, A. Jongsma, I.M. deLeeuw, F. Innings, and S. Heinrich, "Fluidization characteristics of cohesive powders in vibrated fluidized bed drying at low vibration frequencies," *Powder Technol.*, **357** 54–63 (2019). doi:10.1016/j.powtec.2019.08.105.

51) L. Meili, R.V. Daleffe, and J.T. Freire, "Fluid dynamics of fluidized and vibrofluidized beds operating with geldart c particles," *Chem. Eng. Technol.*, **35** (*9*) 1649–1656 (2012). doi:10.1002/ceat.201100546.

52) C.G.J. Baker, A.R. Khan, Y.I. Ali, and K. Damyar, "Simulation of plug flow fluidized bed dryers," *Chem. Eng. Process. Process Intensif.*, **45** (*8*) 641–651 (2006). doi:10.1016/j.cep.2006.01.008.

53) L. Nilsson, and R. Wimmerstedt, "Residence time distribution and particle dispersion in a longitudinal-flow fluidized bed," *Chem. Eng. Sci.*, **43** (*5*) 1153–1160 (1988). doi:10.1016/0009-2509(88)85075-9.

54) L. Nilsson, "Influence of solids dispersion on the heat transfer process in a longitudinal-flow fluidized bed," *Chem. Eng. Sci.*, **43** (*12*) 3217–3223 (1988). doi:10.1016/0009-2509(88)85129-7.

55) A.S. Mujumdar, ed., "Handbook of Industrial Drying," 3rd ed., CRC Press, Boca Raton, 2006. doi:10.1201/9781420017618.

56) S. Syahrul, I. Dincer, and F. Hamdullahpur, "Thermodynamic modeling of fluidized bed drying of moist particles," *Int. J. Therm. Sci.*, **42** (*7*) 691–701 (2003). doi:10.1016/S1290-0729(03)00035-8.

57) Q. Tu, Z. Ma, and H. Wang, "Investigation of wet particle drying process in a fluidized bed dryer by cfd simulation and experimental measurement," *Chem. Eng. J.*, **452** 139200 (2023). doi:10.1016/j.cej.2022.139200.

58) E. Tsotsas, "M6 Heat Transfer from a Wall to Stagnant and Mechanically Agitated Beds," in: VDI

Heat Atlas, Springer, Berlin, Heidelberg, 2010: pp. 1311–1326. doi:10.1007/978-3-540-77877-6_99.

59) E. Saniso, S. Prachayawarakorn, T. Swasdisevi, and S. Soponronnarit, "Parboiled rice production without steaming by microwave-assisted hot air fluidized bed drying," *Food Bioprod. Process.*, **120** 8–20 (2020). doi:10.1016/j.fbp.2019.12.005.

60) Y. Yan, B. Qi, W. Zhang, X. Wang, and Q. Mo, "Investigations into the drying kinetics of biomass in a fluidized bed dryer using electrostatic sensing and digital imaging techniques," *Fuel*, **308** 122000 (2022). doi:10.1016/j.fuel.2021.122000.

61) T. Ichise, and Y. Tatemoto, "Numerical analysis of drying characteristics of frozen material immersed in fluidized bed at low temperature under reduced pressure," *Adv. Powder Technol.*, **33** (*8*) 103661 (2022). doi:10.1016/j.apt.2022.103661.

62) B. Paudel, and Z.-G. Feng, "Prediction of minimum fluidization velocity for binary mixtures of biomass and inert particles," *Powder Technol.*, **237** 134–140 (2013). doi:10.1016/j.powtec.2013.01.031.

63) S. Zarekar, A. Bück, M. Jacob, and E. Tsotsas, "Reconsideration of the hydrodynamic behavior of fluidized beds operated under reduced pressure," *Powder Technol.*, **Complete** (*287*) 169–176 (2016). doi:10.1016/j.powtec.2015.09.027.

64) K. Kusakabe, T. Kuriyama, and S. Morooka, "Fluidization of fine particles at reduced pressure," *Powder Technol.*, **58** (*2*) 125–130 (1989). doi:10.1016/0032-5910(89)80024-5.

65) D.J. Gunn, "Transfer of heat or mass to particles in fixed and fluidised beds," *Int. J. Heat Mass Transf.*, **21** (*4*) 467–476 (1978). doi:10.1016/0017-9310(78)90080-7.

66) R. Clift, J.R. Grace, and M.E. Weber, "Bubbles, Drops, and Particles," Courier Corporation, 2005.

67) T.H. Chilton, and A.P. Colburn, "Mass transfer (absorption) coefficients prediction from data on heat transfer and fluid friction," *Ind. Eng. Chem.*, **26** (*11*) 1183–1187 (1934). doi:10.1021/ie50299a012.

68) S.W. Churchill, and H.H.S. Chu, "Correlating equations for laminar and turbulent free convection from a horizontal cylinder," *Int. J. Heat Mass Transf.*, **18** (*9*) 1049–1053 (1975). doi:10.1016/0017-9310(75)90222-7.

69) H.A. Vreedenberg, "Heat transfer between a fluidized bed and a horizontal tube," *Chem. Eng. Sci.*, **9** (*1*) 52–60 (1958). doi:10.1016/0009-2509(58)87007-4.

70) M.J. Rhodes, "Introduction to Particle Technology," John Wiley & Sons, 2008.

71) X. Sukunza, A. Pablos, M. Tellabide, I. Estiati, F.B. Freire, R. Aguado, and M. Olazar, "A model for predicting the performance of a batch fountain confined spouted bed dryer at low and moderate temperatures," *Powder Technol.*, **405** 117506 (2022). doi:10.1016/j.powtec.2022.117506.

72) L. Spreutels, F. Debaste, R. Legros, and B. Haut, "Experimental characterization and modeling of baker's yeast pellet drying," *Food Res. Int.*, **52** (*1*) 275–287 (2013). doi:10.1016/j.foodres.2013.02.038.

73) Y. Shao, B. Ren, B. Jin, W. Zhong, H. Hu, X. Chen, and C. Sha, "Experimental flow behaviors of irregular particles with silica sand in solid waste fluidized bed," *Powder Technol.*, **234** 67–75 (2013). doi:10.1016/j.powtec.2012.09.019.

74) S. Zarekar, A. Bück, M. Jacob, and E. Tsotsas, "Numerical study of the hydrodynamics of fluidized beds operated under sub-atmospheric pressure," *Chem. Eng. J.*, **372** 1134–1153 (2019). doi:10.1016/j.cej.2019.04.159.

75) D.D.W. Green, and D.M.Z. Southard, "Perry's Chemical Engineers' Handbook," McGraw-Hill Education, 2019. https://www.accessengineeringlibrary.com/content/book/9780071834087 (accessed November 22, 2022).

76) H.G. Wang, W.Q. Yang, P. Senior, R.S. Raghavan, and S.R. Duncan, "Investigation of batch fluidized-bed drying by mathematical modeling, cfd simulation and ect measurement," *AIChE J.*, **54** (*2*) 427–444 (2008). doi:10.1002/aic.11406.

77) B. Paláncz, "A mathematical model for continuous fluidized bed drying," *Chem. Eng. Sci.*, **38** (*7*) 1045–1059 (1983). doi:10.1016/0009-2509(83)80026-8.

78) C. van den Berg, and S. Bruin, "WATER ACTIVITY AND ITS ESTIMATION IN FOOD SYSTEMS: THEORETICAL ASPECTS," in: L.B. Rockland, G.F. Stewart (Eds.), Water Act. Influ. Food Qual., Academic Press, 1981: pp. 1–61. doi:10.1016/B978-0-12-591350-8.50007-3.

79) F. Debaste, V. Halloin, L. Bossart, and B. Haut, "A new modeling approach for the prediction of yeast drying rates in fluidized beds," *J. Food Eng.*, **84** (*2*) 335–347 (2008). doi:10.1016/j.jfoodeng.2007.05.022.

80) E.J. Quirijns, A.J. van Boxtel, W.K. van Loon, and G. van Straten, "Sorption isotherms, gab parameters and isosteric heat of sorption," *J. Sci. Food Agric.*, **85** (*11*) 1805–1814 (2005). doi:10.1002/jsfa.2140.

81) I. Dincer, "On energetic, exergetic and environmental aspects of drying systems," *Int. J. Energy Res.*, **26** (*8*) 717–727 (2002). doi:10.1002/er.792.

82) J.A. Almendros-Ibáñez, M. Díaz-Heras, J.F. Belmonte, and C. Sobrino, "Exergy analysis of packed and fluidized bed thermal energy storage systems," *Appl. Therm. Eng.*, **241** 122436 (2024). doi:10.1016/j.applthermaleng.2024.122436.

83) W.B. Wincy, M. Edwin, and S.J. Sekhar, "Exergetic evaluation of a biomass gasifier operated reversible flatbed dryer for paddy drying in parboiling process," *Biomass Convers. Biorefinery*, **13** (*5*) 4033–4045 (2023). doi:10.1007/s13399-021-01322-2.

84) E. Özahi, and H. Demir, “A model for the thermodynamic analysis in a batch type fluidized bed dryer,” *Energy*, **59** 617–624 (2013). doi:10.1016/j.energy.2013.07.001.

85) S. Syahrul, F. Hamdullahpur, and I. Dincer, “Exergy analysis of fluidized bed drying of moist particles,” *Exergy Int. J.*, **2** (*2*) 87–98 (2002). doi:10.1016/S1164-0235(01)00044-9.

86) M. Mohseni, A. Kolomijtschuk, B. Peters, and M. Demoulling, “Biomass drying in a vibrating fluidized bed dryer with a lagrangian-eulerian approach,” *Int. J. Therm. Sci.*, **138** 219–234 (2019). doi:10.1016/j.ijthermalsci.2018.12.038.

87) S. Taheri, G. Brodie, and D. Gupta, “Microwave fluidised bed drying of red lentil seeds: drying kinetics and reduction of botrytis grey mold pathogen,” *Food Bioprod. Process.*, **119** 390–401 (2020). doi:10.1016/j.fbp.2019.11.001.

88) H.J. Das, P. Mahanta, R. Saikia, and M.S. Aamir, “Performance evaluation of drying ccharacteristics in conical bubbling fluidized bed dryer,” *Powder Technol.*, **374** 534–543 (2020). doi:10.1016/j.powtec.2020.06.051.

89) X. Zhu, Z. Zhang, L.M. Hinds, D.-W. Sun, and B.K. Tiwari, “Applications of ultrasound to enhance fluidized bed drying of ascophyllum nodosum: drying kinetics and product quality assessment,” *Ultrason. Sonochem.*, **70** 105298 (2021). doi:10.1016/j.ultsonch.2020.105298.

90) H. Chen, S. Rustagi, E. Diep, T.A.G. Langrish, and B.J. Glasser, “Scale-up of fluidized bed drying: impact of process and design parameters,” *Powder Technol.*, **339** 8–16 (2018). doi:10.1016/j.powtec.2018.07.087.

91) H. Perazzini, F.B. Freire, and J.T. Freire, “The influence of vibrational acceleration on drying kinetics in vibro-fluidized bed,” *Chem. Eng. Process. Process Intensif.*, **118** 124–130 (2017). doi:10.1016/j.cep.2017.04.009.

92) B. Lan, P. Zhao, J. Xu, B. Zhao, M. Zhai, and J. Wang, “CFD-dem-ibm simulation of particle drying processes in gas-fluidized beds,” *Chem. Eng. Sci.*, **255** 117653 (2022). doi:10.1016/j.ces.2022.117653.

93) C. Si, J. Wu, Y. Zhang, G. Liu, and Q. Guo, “Experimental and numerical simulation of drying of lignite in a microwave-assisted fluidized bed,” *Fuel*, **242** 149–159 (2019). doi:10.1016/j.fuel.2019.01.002.

94) L. Zhu, Z. Zhao, C. Liu, W. Li, Y. Zhang, Y. Zhang, C. Zheng, K. Luo, and X. Gao, “CFD-dem simulations of a fluidized bed with droplet injection: effects on flow patterns and particle behavior,” *Adv. Powder Technol.*, **34** (*1*) 103897 (2023). doi:10.1016/j.apt.2022.103897.

95) J. Yan, H. Wei, Z. You, H. Wu, X. Xu, and H. Xie, “Energetic and exergetic performances during drying of freshly harvested peanut with industrial mixed-flow dryer,” *Energy Rep.*, **8** 7457–7467 (2022). doi:10.1016/j.egyr.2022.05.252.

96) D. Chaatouf, M. Salhi, B. Raillani, S. Amraqui, A. Mezrhab, and H. Naji, “Parametric analysis of a sensible heat storage unit in an indirect solar dryer using computational fluid dynamics,” *J. Energy Storage*, **49** 104075 (2022). doi:10.1016/j.est.2022.104075.

97) M. Khanali, S. Rafiee, A. Jafari, and S.H. Hashemabadi, “Experimental investigation and modeling of plug-flow fluidized bed drying under steady-state conditions,” *Dry. Technol.*, **31** (*4*) 414–432 (2013). doi:10.1080/07373937.2012.738751.

98) W. Cai, X. Xia, X. Li, X. Chen, Z. Xu, and H. Lu, “Transition fluidization in pulsating subcritical water fluidized beds,” *Chem. Eng. Res. Des.*, **184** 488–500 (2022). doi:10.1016/j.cherd.2022.06.024.

99) J. Su, C. Zhou, X. Jiang, and Z. Qiao, “Orderly arrangement of agricultural biomass particles in designed gas–solid fluidized beds using cfd-dem and image experiment,” *Comput. Electron. Agric.*, **204** 107510 (2023). doi:10.1016/j.compag.2022.107510.

100) H.Q. Che, D. Liu, W.B. Tian, S. Gao, J.T. Sun, and L.J. Xu, “CFD-dem study of gas-solid flow regimes in a wurster type fluidized bed with experimental validation by electrical capacitance tomography,” *Chem. Eng. J.*, **389** 124280 (2020). doi:10.1016/j.cej.2020.124280.

101) W. Cai, X. Kong, Q. Ye, L. Wang, D. Ren, and H. Lu, “Numerical modelling of hydrodynamics of molten salt fluid-particles fluidized beds using cfd-dem and tfm approaches,” *Powder Technol.*, **410** 117882 (2022). doi:10.1016/j.powtec.2022.117882.